2008-07-09

Mode I Fracture Toughness Testing of Friction Stir Processed HSLA-65

Jeffery D. Horschel
Brigham Young University - Provo

MODE ONE FRACTURE TOUGHNESS TESTING OF FRICTION STIR PROCESSED HSLA-65

by

Jeffery D. Horschel

A thesis submitted to the faculty of

Brigham Young University

in partial fulfillment of the requirements for the degree of

Master of Science

Department of Mechanical Engineering

Brigham Young University

August 2008

BRIGHAM YOUNG UNIVERSITY

GRADUATE COMMITTEE APPROVAL

of a thesis submitted by

Jeffery D. Horschel

This thesis has been read by each member of the following graduate committee and by majority vote has been found to be satisfactory.

Date	Tracy W. Nelson, Chair
Date	Carl D. Sorensen
Date	Michael P. Miles

BRIGHAM YOUNG UNIVERSITY

As chair of the candidate's graduate committee, I have read the thesis of Jeffery D. Horschel in its final form and have found that (1) its format, citations, and bibliographical style are consistent and acceptable and fulfill university and department style requirements; (2) its illustrative materials including figures, tables, and charts are in place; and (3) the final manuscript is satisfactory to the graduate committee and is ready for submission to the university library.

Date

Tracy W. Nelson
Chair, Graduate Committee

Accepted for the Department

Matthew R. Jones
Graduate Coordinator

Accepted for the College

Alan R. Parkinson
Dean, Ira A. Fulton College of Engineering and Technology

ABSTRACT

MODE ONE FRACTURE TOUGHNESS TESTING OF

FRICTION STIR PROCESSED HSLA-65

Jeffery D. Horschel

Department of Mechanical Engineering

Master of Science

In order to investigate the viability of friction stir welding for use in Naval construction, mode one elastic-plastic fracture toughness of friction stir processed HSLA-65 was determined using current ASTM 1820 and BS 7448 standards. Double-sided welds were used to achieve 12.7 mm thick samples. A constant feed rate of 100 mm/min was used for all welds. To explore the effect of weld parameters on toughness, welds were produced using two rotational speeds: 340 RPM and 490 RPM. The weld centerline, advancing side hardened region (ASHR), and TMAZ/HAZ regions were sampled, in addition to un-welded parent material. All elastic-plastic fracture toughness values were thickness dependent. For welds produced at 340 RPM, toughness ranged from 33% to 75% below parent material. By increasing the rotational speed to 490 RPM, weld toughness was likewise less

than the parent material, but increased 12% to 50% relative to welds produced at 340 RPM. The lowest measured toughness was in the ASHR samples for both parameters. This region of the weld exhibited mixed mode stress-strain conditions and toughness 75% and 62% less than parent material. Toughness values for all samples failed to meet qualification requirements of both ASTM 1820 and BS 7448 due to non-uniform crack extension. Irregular crack extension was caused by the through thickness change in tensile properties due to welding and the affect this had on the plastic zone size compared to the thickness. Increased weld toughness from 340 RPM to 490 RPM was attributed to microstructural differences as a result of increased rotational speed. In addition, higher crack extensions were observed in the second weld pass relative to the first for both rotational speeds. This was attributed to weld tempering of the first pass by the second. The ASHR samples exhibited the highest crack extensions. In this location, the weld microstructure consisted of Widmanstatten ferrite, a microstructure known to be detrimental to toughness.

ACKNOWLEDGMENTS

I would like to first thank my wife, Elizabeth, for her support, love, and the sacrifices she has made to allow me to do this work; as well as my children. I would also like to thank my parents, Dan and Janice, for their example, inspiration, hard work, and unceasing motivation; who have also given me many an opportunity, including this one.

I would also like to thank my committee members, especially Dr. Nelson, for their advice, patience, involvement, and excitement with this work.

I also want to thank all those in the Friction Stir Research Lab who have given of themselves to help in the completion of this work, as well as making it light. I would also like to recognize Annette for her encouragement and advice. Additionally, the patience of Boy Scout Troops 727 and 923, and all those associated with them, is duly recognized and appreciated. Also, appreciation is extended to coworkers at Cessna Aircraft Company and friends at WSU that have given of their time and resources allowing me to complete this work.

TABLE OF CONTENTS

LIST OF TABLES

LIST OF FIGURES

1 Introduction

1.1 Background

Since its inception, friction stir welding has been examined for use in many different damage tolerant designs. For example, friction stir welding has been proposed as a substitute for riveting in aerospace structures [1]. Also, with the development of advanced friction stir welding tools [2], high strength steels can now be friction stir welded. As such, friction stir welding has gained interest among the pipeline and shipbuilding industries, particularly the Navy's HSLA (high strength low alloy) program. Initiated in 1980, this program was developed to find ways to accomplish the goal of reducing "shipbuilding costs through improvement of welding processes, materials, technologies, procedures, and techniques, while simultaneously improving quality, strength, and toughness of hull steels [3]."

The interest in friction stir welding stems from the seemingly superior post weld mechanical properties produced by the friction stir welding process compared to conventional welding processes. This in and of itself presents the problem: while traditional joining techniques have been well understood for decades, friction stir welding is relatively new and imposes its own set of challenges regarding its use. In respect to the aerospace, pipeline, and shipbuilding industries, damage tolerant design (or a design that will withhold its integrity with the presence of flaws or cracks) is of great importance. Even so, little is known about the fracture properties of friction stir welds, and whether a

friction stir welded structure is economical as well as damage tolerant. Widespread implementation of friction stir welding in structures is subject to understanding the toughness properties of the welded material.

1.2 Fracture Toughness Testing

The fracture properties of friction stir welded HSLA steels have not been extensively explored. While many standards exist that delineate the proper fracture toughness testing of homogeneous materials and even traditional arc welds, there is little literature addressing the application of these standards to friction stir welds.

1.2.1 Homogeneous Materials

In homogeneous materials, compact tension specimens are cut from the material with a starter notch in the area of the material where the fracture toughness is to be evaluated. These specimens are then cyclically loaded to grow a crack in the bottom of the notch (called a precrack). At this point, the test procedure varies for K_{IC} (elastic) and J_{IC} (elastic-plastic) evaluations. For K_{IC}, a tensile load on the specimen is ramped up until fast fracture occurs, while recording the load and crack opening displacement. For J_{IC}, specimens are cyclically loaded to produce stable crack growth while recording the displacement of the load line, crack extension, and load for each cycle. Analysis of the records following prescribed procedures [4,5] will produce either qualified (or thickness dependent) K_C or J_C values or valid plane strain fracture toughness K_{IC} or J_{IC} values.

1.2.2 Arc Welds

Toughness is determined in a similar manner for traditional weld specimens. However, due to the heterogeneity of the weld, careful placement of the starter notch/fatigue precrack and post-test sectioning are crucial to the determining of fracture toughness values of microstructurally distinct zones of a weldment. For example, in a multi-pass arc weld process, many distinct regions of material are produced, each with different properties. Local brittle zones exist in the coarse-grain HAZ (CGHAZ). Because this is a region of low toughness and since it causes failure in a weak link fashion, it is imperative to know the fracture toughness of this region if it is to be used in a structural setting. Testing the fracture toughness of a specific region requires that "the precrack must be located close enough to the weak link that the crack-tip process zone can initiate fracture" [6]. In conjunction with this idea is the subsequent verification that the fatigue crack did indeed sample the weld region in question, and a quantification of how much sampling took place. By this process the toughness of various weld regions of a traditional weld can be determined.

1.2.3 Fracture Toughness Testing of Friction Stir Welds

The challenge that friction stir welding poses is two-fold: 1) while traditional welding techniques can be done in material of any thickness, friction stir welding is limited to producing relatively thin specimens, especially for tough materials like HSLA-65; and 2) like traditional welding techniques, adequate control of the position, orientation, and containment (i.e. prevention of out-of-plane cracking) of the starter notch, fatigue precrack, and any subsequent crack growth during testing is imperative to the successful determination of toughness for a given region of weld material.

As far as evaluating the fracture toughness of friction stir welds in HSLA steels, there is no literature available. However, the aerospace industry is just as interested in utilizing friction stir welding on aircraft for the same reasons shipbuilders want to use it on vessels. Therefore, a number of fracture toughness evaluations of friction stir welds in aluminum have been published by the aerospace community. Jata et al successfully tested eccentrically loaded single edge tension samples for fatigue crack growth rates in the weld nugget and HAZ of 7050 [7]. Sutton et al showed that the crack tip opening displacement (CTOD) is a viable means of measuring the fracture response of friction stir welded 2024 [8]. He was also able to demonstrate the affect of heat input on CTOD, and that hardness and microstructure affected crack propagation. While these papers glean little information on the toughness properties of friction stir welded HSLA steels, they do offer insights into approaching fracture toughness testing of friction stir welds.

1.3 Friction Stir Welded HSLA-65

While traditional multi-pass arc welding techniques produce well defined boundaries between HAZ and weld nugget regions, friction stir welding sometimes does not. Figure 1-1 is a photo of the weld zone of friction stir processed HSLA-65. While some boundaries are clear, perhaps between the TMAZ and the hardened region, other boundaries are not as apparent. For example, the boundary between the TMAZ and the HAZ is very gradual. Likewise, the transition from the hardened region to the nugget is equally indistinct. Varying the weld parameters also changes the size and shape of each region. Proper characterization of these different regions is critical to ensuring the successful placement of the starter notch to ensure the crack samples the desired region.

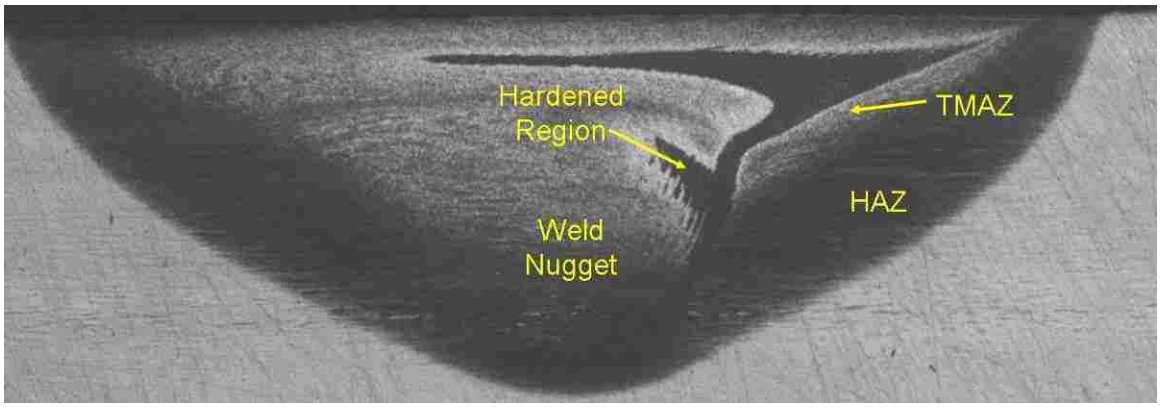

Figure 1-1: Photo of the different zones of weld material in HSLA-65: weld nugget, hardened region, TMAZ, and HAZ.

Since friction stir welding produces regions of material oblique to the thickness (and crack plane), it is difficult to guarantee that a crack maintains a path in a desired plane. While this is the case of friction stir welds in any material, not just HSLA-65, many institutions have demonstrated successful crack containment by utilizing specimen designs outlined by ASTM standards. In fact, the Navy, in conducting toughness tests, implements side grooves (a procedure outlined in ASTM standards) to increase crack constraint.

HSLA-65 is sensitive to the Hall-Petch effect, or the strengthening of a material by decreasing the grain size. Since friction stir welding produces a region of very fine grain structure, the weak link may be the parent material itself. Preliminary tensile tests conducted at BYU on friction stir processed X-65 have demonstrated ductile overload failure in the base metal. While this indicates a clearly *strengthened* weld region, it is no indication of the *toughness* of the weld region.

In addressing the issue of toughness, Charpy v-notch tests done at Oak Ridge National Labs [9] on friction stir welded HSLA-65 suggest a tougher and stronger weld

region. The same tests conducted by Konkol et al [10] showed "the CVN toughness in the stir zone is significantly lower than that of the HSLA plate; however, it was higher than the specified plate minimum. The stir-zone toughness is also higher than the specified minimum for the MIL-71T1 flux-cored arc weld metal typically used to join HSLA steel." While these tests have addressed specifically toughness of friction stir welded HSLA-65, they do not agree, and provide little insight as what to expect.

1.4 Problem Statement

Providing safe damage tolerant designs of structures utilizing friction stir welding as a primary joining technique implies understanding the fracture characteristics of the material joined or processed by friction stir welding. However, a procedure for obtaining that understanding is still a relatively untouched subject and requires attention if the goal of damage tolerant designs of friction stir welded structures is to be obtained.

2 Experimental Method

2.1 General Approach

Friction stir welding is currently limited to producing welds much thinner than the thickness required to produce plane strain conditions in HSLA-65. Therefore, this thesis is limited to qualified (thickness dependent) toughness values only. This was done under the assumption that since base metal HSLA-65 needs to be approximately 60 mm thick to impose plane strain conditions at a crack tip at room temperature, anything thinner will always "leak before break." Equally, since Charpy v-notch tests done by Feng [9] and Konkol [10] hinted that toughness ranged from better than arc welding to better than base metal, friction stir welded HSLA-65 should at least meet minimum weld standards, and also "leak before break." This thesis attempted to quantitatively determine the toughness of friction stir welds in relation to arc-weld and parent material toughness by comparing the elastic-plastic fracture toughness of friction stir welded material to parent material for specimens of similar thickness. Therefore, fracture toughness tests were conducted according to ASTM 1820 and British Standard 7448 in 12.7 mm thick base metal sheet HSLA-65 and then in friction stir processed HSLA-65 of the same thickness.

2.2 Welding

2.2.1 Machine and Tooling

Welding was conducted at Brigham Young University with a Transformation Technologies Inc. friction stir welder capable of welding 3 m lengths. The machine is computer controlled, and is easily programmed using MegaStir Technologies' computer interface. The welding tool was a CS4 (Convex-Step Spiral-Scrolled Shoulder) design made of a PCBN insert locked to a tungsten carbide shank. Details of this tool are included in Appendix A. This tool design was chosen because of its exceptional tool life, excellent tool path surface finish, and improved stirring of the weld material. The pin length was designed such that overlap between the top and bottom weld passes was achieved in the desired plate thickness. The tool was cooled via circulating coolant through the tool holder during welding and argon gas shielding was used to prevent oxidation of the tool and weld surface.

2.2.2 Material and Weld Parameters

HSLA-65 is a High Strength Low Alloy steel (typically classified as having less than 0.1% carbon content) used extensively in US Naval construction. The development of this alloy is in response to welding difficulties (typically low toughness) and costs associated with previous HY steels. The reduction of carbon content results in a lower strength steel, but yields better toughness. In order to recover strength, small amounts of carbide forming elements that control grain growth are added (Table 2-1) which cause strengthening by refinement of the microstructure. The effect of reducing microstructure size to increase strength is also known as the Hall-Petch effect. The resulting base metal

microstructure consists of polygonal ferrite, interspersed with small regions of bainite or martensite (Figure 2-1).

Table 2-1: Percent composition of various elements in HSLA-65 sheet used.

Element	%	Element	%
Carbon	0.081	Copper	0.26
Manganese	1.43	Nitrogen	0.009
Silicon	0.2	Vanadium	0.055
Sulfur	0.003	Titanium	0.013
Phosphorus	0.022	Niobium	0.021
Nickel	0.35	Aluminum	0.018
Molybdenum	0.063	Boron	<.0005
Chromium	0.15	Oxygen	0.003

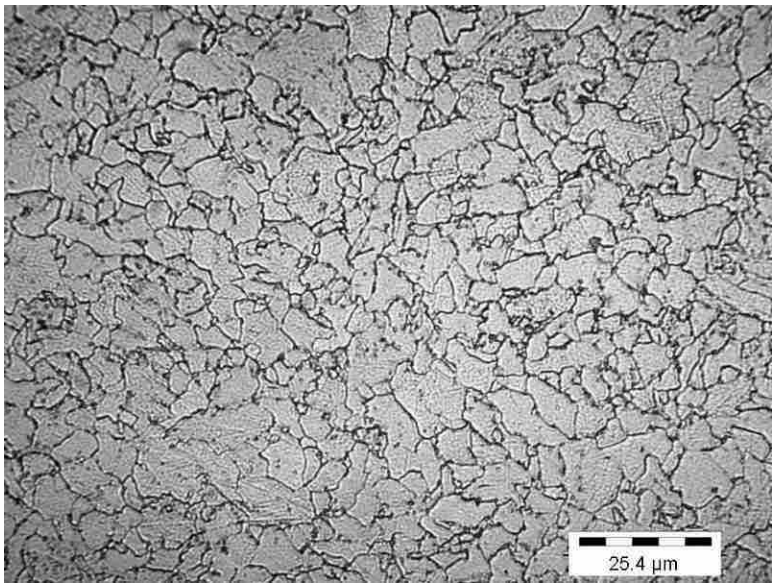

Figure 2-1: Micrograph showing microstructure of base metal HSLA-65 material.

To validate the test procedure and to explore dependence of toughness on weld parameters, two different weld parameters were explored (Table 2-2). The change in parameters was done systematically: from weld set A to weld set B, the rotational speed

was increased. This was done in order to attribute any changes in toughness to a change in rotational speed.

Table 2-2: Weld parameters.

	Feed-Rate mm/min	Rotational Speed RPM	Vertical Force kN	Weld Power W	Heat Input J/mm
Weld A	100	340	42.3	4373	2583
Weld B	100	490	33.4	4321	2552

Weld power was calculated using Equation (1), the spindle torque, and spindle RPM [11].

$$\text{Weld Power} = \frac{(2\pi)\Omega M}{60} \quad \textbf{(1)}$$

Where Ω is the spindle speed in RPM, and M is the torque (N-m). Torque was calculated by averaging the spindle torque recorded for the duration of each weld. Once weld power was calculated, Equation (2) was utilized to calculate the heat input [11].

$$\text{Heat Input} = \frac{P.I.}{v} \quad \textbf{(2)}$$

Where P.I. is the weld power (W) and v is the feed rate (mm/sec).

'Welds' were actually friction stir processed with a two pass (top and bottom) force controlled process in order to generate the desired thickness. Welds were conducted in opposite directions on the top and bottom to assure weld features overlap (i.e. the advancing side of top weld overlaps the advancing side of the bottom weld). The plates were welded in the longitudinal direction, parallel to the rolling direction.

2.2.3 Weld Qualification

Weld parameters were arrived at by running practice welds at various parameters and subsequently checking for defects using dye penetrant inspection. Once defect free welds were obtained, plates were welded and transverse sections were cut, polished, etched, and inspected using visual microscopy to again ensure full healing of the weld. Also, these same etched sections were used for determining notch placement and hardness mapping of the welds.

2.3 Sample Design

Compact tension samples were used for all fracture toughness evaluations. Samples were designed to have a nominal thickness (B) of 12.7 mm and a nominal width (W) of 51 mm. This corresponds to a W/B = 4 for specimens with $B \leq 12.7$ mm as outlined by ASTM 1820 (sections 6.5.2.2 and 7.3) and BS 7448. However, machining operations prior to welding, between weld passes, and post weld reduced the thickness to between 11.07 mm and 11.43 mm. The difference between maximum and minimum thickness was 0.36 mm, well within the ±0.508 mm tolerance called out by the standards. However, the width-to-thickness ratio was 4.44; greater than the maximum allowed by the standards. Nonetheless, the standards point out that any thickness can be used, as long as the qualification requirements are met [4].

Preliminary tests in base metal material indicated a need for side grooves along the crack plane on both sides of the sample to increase crack constraint. These were included in the final design of all samples. Also, integral knife edges at the load line

were included in the design of the sample to allow installation of a COD gauge. A detailed drawing of the compact tension sample is included in Appendix B.

2.3.1 Notch Placement and Verification

Placement of notches was determined by first performing hardness maps across a transverse section of each weld. Hardness maps in Figure 2-2 and Figure 2-3 were made from discrete hardness measurements spaced 600 microns apart both vertically and horizontally on the sample. Software was then used to interpolate between hardness measurements and create the color image. The results for weld A and B are shown in Figure 2-2.

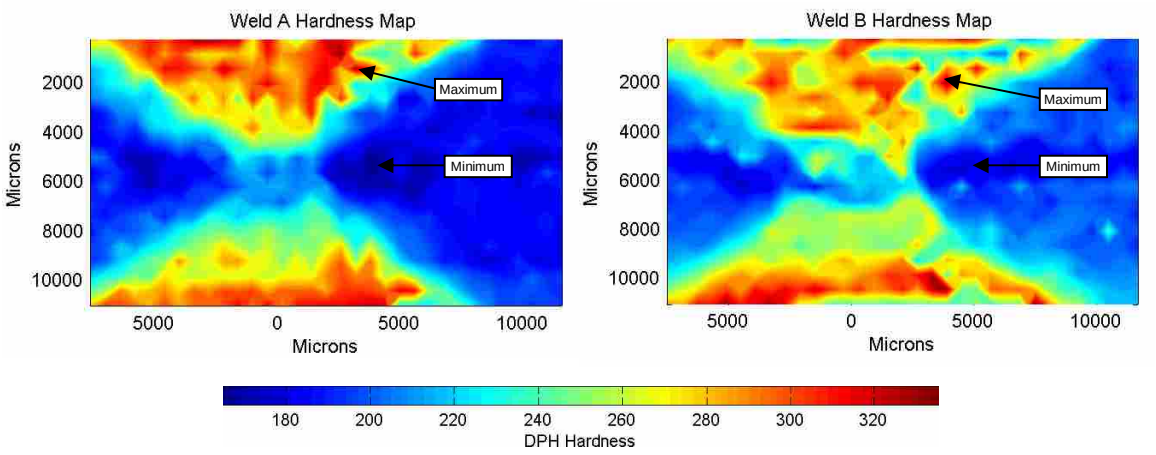

Figure 2-2: Microhardness maps of weld A and weld B.

It was determined from the onset that notch locations would be weld positional as opposed to testing a specific microstructure as per BS 7448 part 2. This means that notches would be placed with respect to a reference position, like the weld centerline. The chosen locations were the weld centerline, the advancing side hardened region, and

the TMAZ/HAZ. In order to locate these features, results from the hardness maps were utilized. Locations of maximum hardness for weld A and B were located at the root of the pin on the advancing side of each weld (Figure 2-2) and were determined to be the location of the advancing side hardened region. The locations of lowest hardness were in a tempered region outside the weld at mid-thickness, and were assumed to be the TMAZ/HAZ. Notches were therefore fabricated in compact tension samples that would drive a crack along these regions. The crack planes are shown as vertical lines in Figure 2-3.

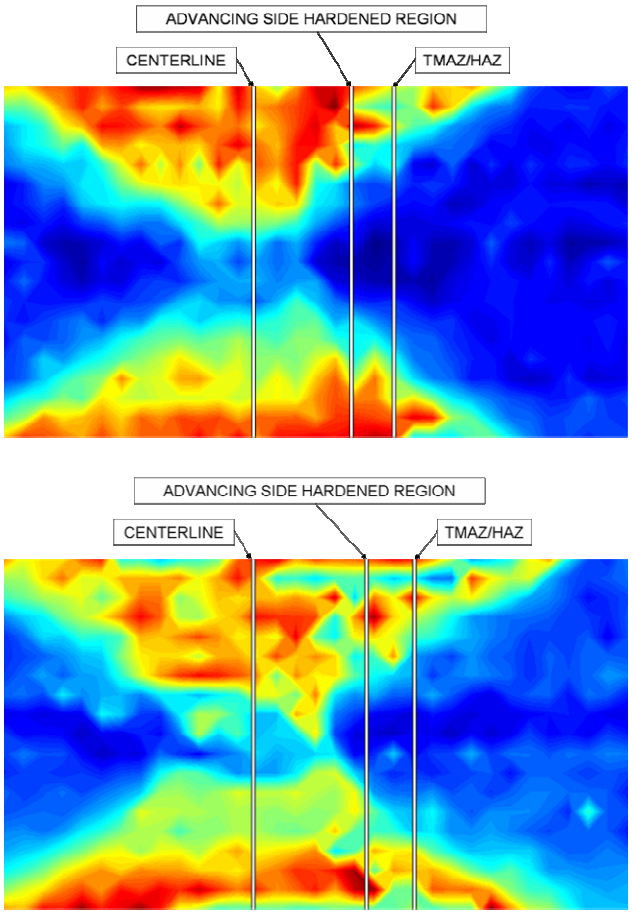

Figure 2-3: Crack planes for weld A (top) and weld B (bottom).

In order to successfully machine the compact tension samples with their notches on the desired plane, the following procedure was utilized. A small reference notch was first machined into the surface of the weld at a known distance from a datum in the parent plate. A transverse sample (that included the reference notch) was then removed from the weld, polished, and etched. Under a microscope, distances were then measured from this reference notch to the centerline, the hardened region on the advancing side, and the advancing side TMAZ/HAZ. These distances, added to the distance to the datum, were then used to machine the compact tension samples with notches in each respective region. Notch placement was later verified by polishing and etching the back face of each side-grooved compact tension sample. These are presented in Figure 2-4.

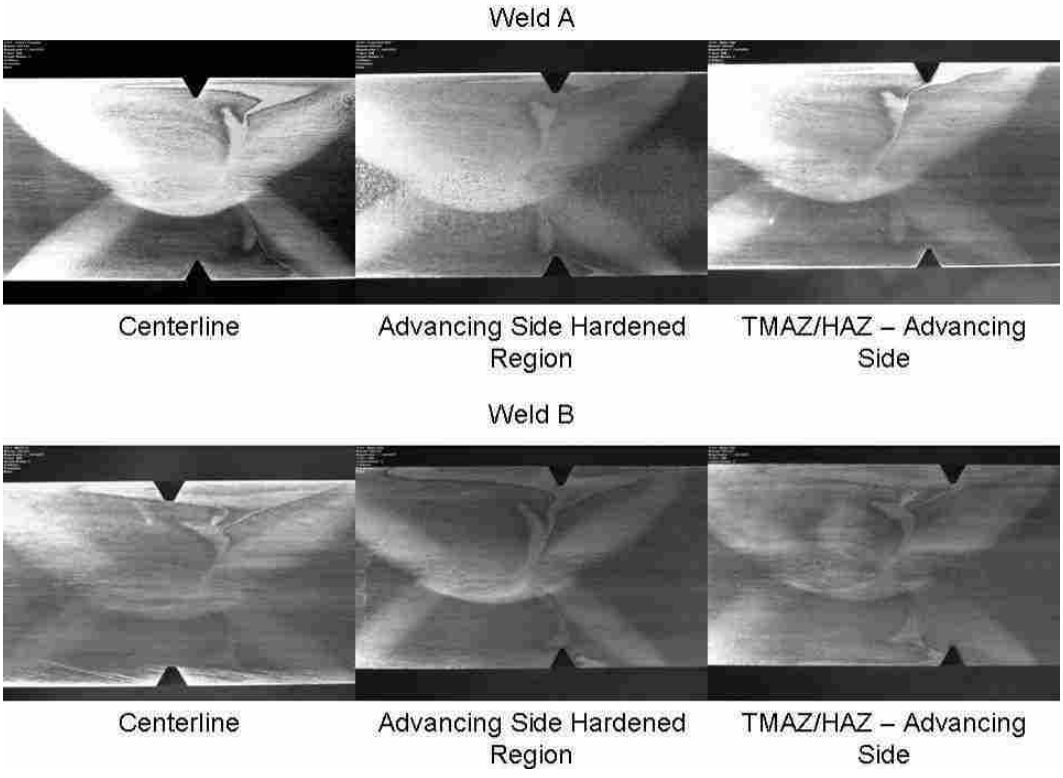

Figure 2-4: Macrographs of polished and etched back faces of compact tension samples showing crack plane placement for both weld A and B. The crack plane is represented by the area of minimum thickness between side grooves.

2.3.2 All Weld Tensile Samples

Additionally, tensile tests of samples made from weld material were also conducted. This was done to acquire yield and ultimate tensile strengths required for calculating J and to gain insight into tensile properties through the thickness of the weld. These were constructed in accordance with ASTM E8 and were sub-size specimens and dimensions. They were also constructed in such a manner that they were made from only welded material. First, a blank was cut in the shape of the profile of a tensile sample longitudinal to and centered on the weld centerline. Slices approximately 1 mm thick were then made (using EDM) through the thickness of the weld until no more samples could be cut.

Tensile tests were conducted for both sets of weld parameters, as well as for base metal. A total of twenty samples were tested: four for base metal and eight for each set of weld parameters. For each sample, the yield and ultimate strengths were recorded. After failure, the distance between a set of marks originally 25.4 mm apart was measured and an estimate of the elongation was also recorded.

During the analysis, it became necessary to obtain estimates of yield strength along each crack plane through the thickness. Tensile samples from the above tests were wide enough to encompass material from multiple crack planes, and tensile data from these samples could not be used as representative of individual crack planes. Therefore, it was required that the through thickness hardness along each crack plane be used to estimate the yield stress. This was done according to published methods [12] and utilized the strain hardening coefficients calculated from the stress-strain records from the above mentioned tensile tests.

2.4 Testing Hardware

All tests (both toughness and tensile) were conducted in laboratory air at room temperature. They were conducted on a servo-hydraulic Instron machine (Figure 2-5). The controller and function generator software was TestarII (version 4.0D). MTS ASTM 1820 fracture toughness testing software was used to program and conduct the toughness aspect of the tests, and initially analyze J-Δa data.

Figure 2-5: Test setup.

An MTS COD gauge was calibrated and installed to measure the load line displacement during testing. Clevises used to load the compact tension samples were manufactured as per ASTM 1820. Additionally, load bearing surfaces were lubricated with anti-seize between uses to reduce friction assuring an accurate measurement of compliance.

2.5 Test Procedure

All toughness tests were conducted in accordance with ASTM 1820 and BS 7448. The general procedure was as follows:

1. Fatigue Pre-Crack
2. Side Groove
3. Obtain J-Δa Data
4. Heat Tint
5. Fatigue to Failure
6. Post-Test Analysis

The results of this procedure produce what is called a resistance curve, or a plot of toughness (J) vs. crack extension (Δa). Analysis of the data divides it into two regions: blunting and crack extension. The initiation toughness is the value of J where blunting transitions to crack extension. In other words, it represents the maximum amount of energy that is removed by deformation at the crack tip from being made available for crack extension. Figure 2-6 shows the qualified initiation toughness, or J_q, is estimated by intersecting of a linear curve fit of J-Δa data with the blunting line. For ASTM 1820 and BS 7448, a power fit of the J-Δa data is intersected with a line parallel to the blunting line and offset by 0.2 mm.

There are a number of methods used to acquire the J-Δa data required for an adequate estimation of the initiation toughness. Figure 2-6 shows three common methods of producing J-Δa data. The data set labeled 'Heat Tint,' is a multiple sample method in which a single sample is loaded and unloaded only once, and crack extension is measured directly after heat tinting and exposing the fracture surface. Therefore, in order to

produce a sufficient J-Δa data, many samples are needed. While this is a time consuming process, it is generally the more accepted method. The other two methods are single sample methods in which a single sample is loaded and unloaded many times, producing many J-Δa pairs. These methods require some way of measuring the crack extension indirectly at each load cycle. The electrical potential method correlates a drop in voltage applied across the sample to crack extension. The elastic compliance method correlates a change in elastic compliance to a crack extension. Figure 2-6 also shows that the initiation value of J_q estimated by each method remains nearly the same.

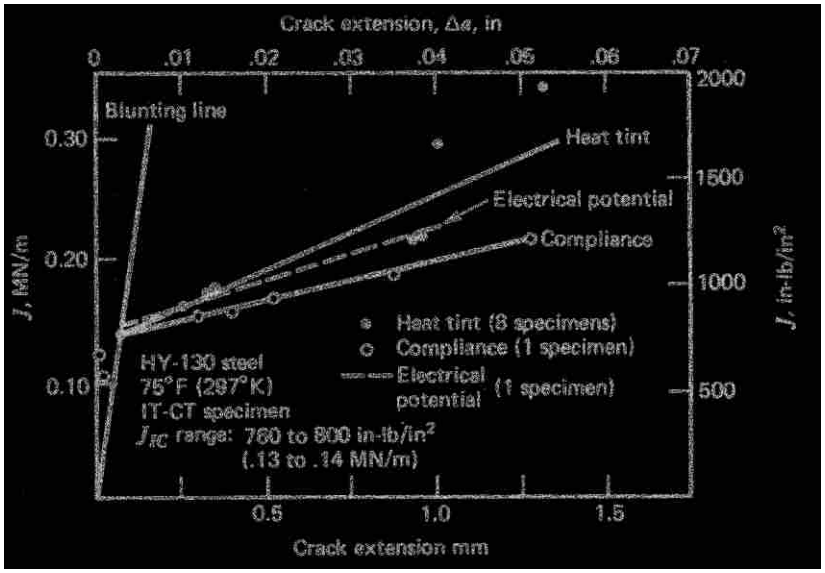

Figure 2-6: Resistance curves produced using three different methods for monitoring crack extension [13].

The elastic compliance method was used to monitor crack extension for all tests in this study. This was done to save time and effort in producing compact tension samples, as only a single sample is required to generate a resistance curve. More importantly, it was chosen because a single specimen test can provide information on

material homogeneity [5]. Since it was known from the onset that the weld is not homogeneous, the results should therefore reflect the non-homogeneity and show which portions of the weld are more susceptible to crack extension. This was an important benefit of using the single sample compliance method, because the primary purpose of this study was to gain a preliminary understanding of the fracture characteristics of friction stir welded HSLA-65; this method provided that information.

While use of the compliance method requires only one sample for generation of a resistance curve, BS 7448 requires three samples to be tested to varying final crack extensions for the generation of a single resistance curve. For each of the three samples, one is tested up to the crack extension limit, another to 50% of the crack extension limit, and a third between a crack extension of 0.1 mm and 0.3 mm. The data from these three samples are then combined. Doing this weights the data towards the transition region between blunting and crack extension when fitted with a power curve, in turn supplying a better estimate of the initiation toughness parameter. It also produces an adequate number of data points within the qualified region, and provides information about the crack front.

Once collected, the J-Δa data must be qualified. General requirements on the test equipment, machining tolerances, fixture alignment, test rate, and temperature must all be within acceptable limits. Since the compliance method is an indirect estimate of the crack extension, it assumes uniform and straight crack extension at each load/unload cycle in order to correlate a change in compliance to crack extension. Therefore, both ASTM 1820 and BS 7448 place requirements on crack front straightness and uniformity, from start to finish, when utilizing the compliance method to estimate crack length and

crack extension. If crack extension is not uniform or straight, the estimate of Δa by this method is inaccurate, as well as any estimate of the initiation toughness from that data. When all these requirements have been met, J_q is calculated and qualified by its own set of requirements. Finally, J_q may qualify as a thickness independent value of fracture toughness, or J_{IC}, if the thickness (B) and original remaining ligament (b_0) are greater than l_{min} calculated in Equation (3).

$$l_{\min} = \frac{25 \cdot J_q}{\sigma_Y} \quad \textbf{(3)}$$

The initiation toughness, J_q, was compared in order to determine quantitative toughness differences between welds and crack plane locations. It was also used to provide initial insight into the stress-strain condition of the crack tip by Equation (3). Furthermore, use of the compliance method to monitor crack extension in heterogeneous weld material provided information into the cracking mechanism and weld weaknesses through analysis of the crack front appearance.

3 Results and Discussion

3.1 Tensile Test Results

Results of the longitudinal all-weld metal tensile tests are shown in Figure 3-1. Both welds A and B exhibit ultimate and yield strength minimums at the mid-thickness of the plate where the two weld passes overlap. In Figure 3-1A, the yield strength in both welds A and B at the mid-thickness are 20% and 9% below that of the base metal, respectively. Within two millimeters of either side of the mid-thickness, the yield strengths in both weld passes exceed the base metal average. Through thickness ultimate strengths in both welds are above the base metal average, shown in Figure 3-1B.

Ultimate and yield strengths in both welds increase from the mid-thickness to a maximum at the weld surfaces. The differences in maximum and minimum yield strength from mid-thickness to the surface are 250 MPa for the first weld pass and 380 MPa for the second weld pass for both welds A and B. These values represent an increase of roughly 45% and 68%, respectively, over base metal. The ultimate strengths in Figure 3-1B are roughly 13% higher at mid-thickness, and increase to a maximum of 35% and 41% at the surface of the first and second weld passes respectively, relative to the base metal.

Tensile elongations, shown in Figure 3-1C, exhibit an inverse relationship to the ultimate and yield strengths. This relationship is shown in Figure 3-1D. Elongations for

both welds were higher in the first weld pass than the second, and weld A was generally higher than weld B.

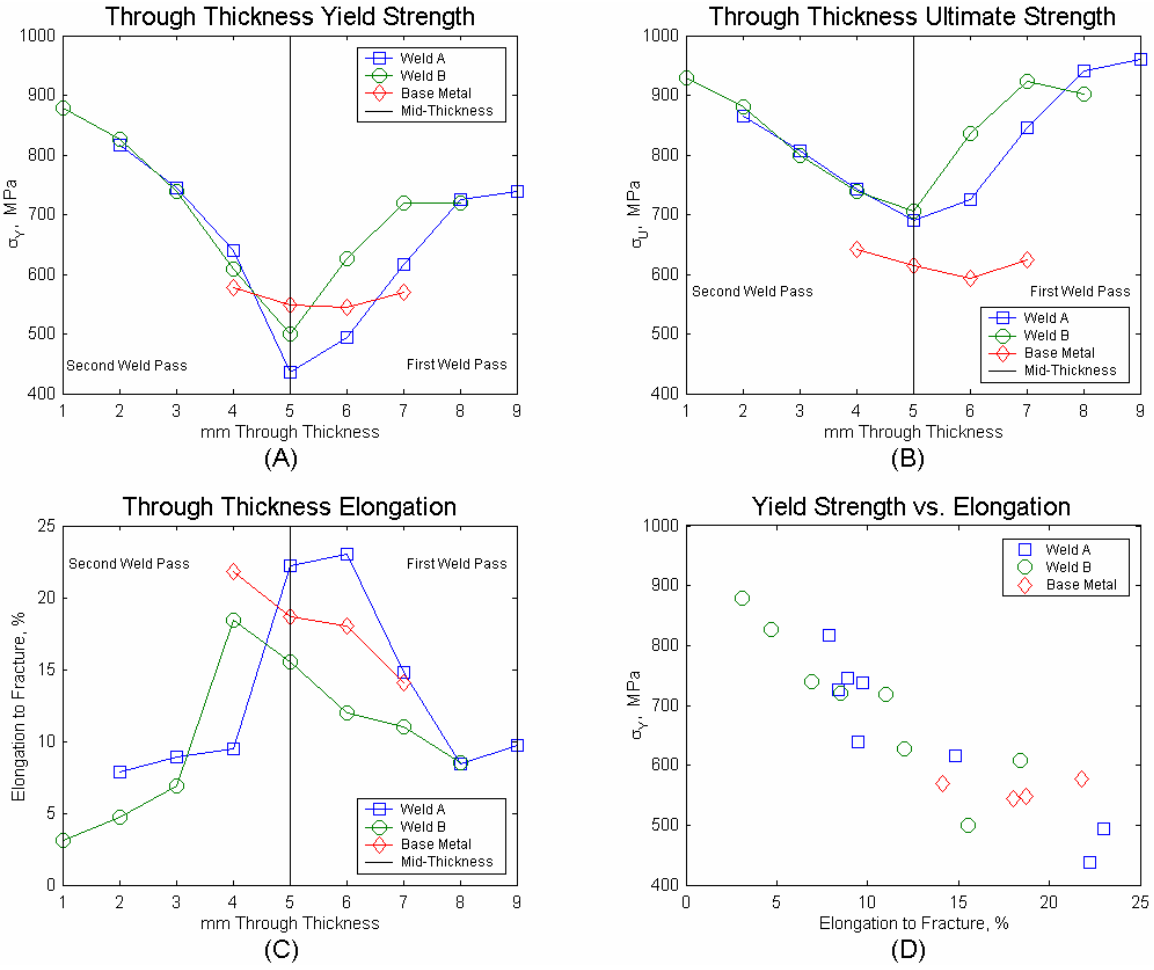

Figure 3-1: Through thickness tensile properties for weld A and B. (A) yield strength, (B) ultimate strength, (C) elongation, and (D) a plot of yield strength versus elongation.

From the data shown in Figure 3-1A and C, it appears that the first weld pass was tempered by the second weld pass. This is evident by reduction in yield strength at the surface of first pass relative to the second pass. Comparing points at 2 mm and 8 mm in Figure 3-1A, weld A exhibits a 11% decrease and weld B a 13% decrease in yield

strength. Similarly, weld A shows a marginal increase of 6% in tensile elongation in the first pass relative to the second, while weld B increases by 45% (Figure 3-1C). This increase in elongation is likely due to weld B being conducted at a higher RPM and the effect this had on the stirred material, since this is the only parameter that changed between welds.

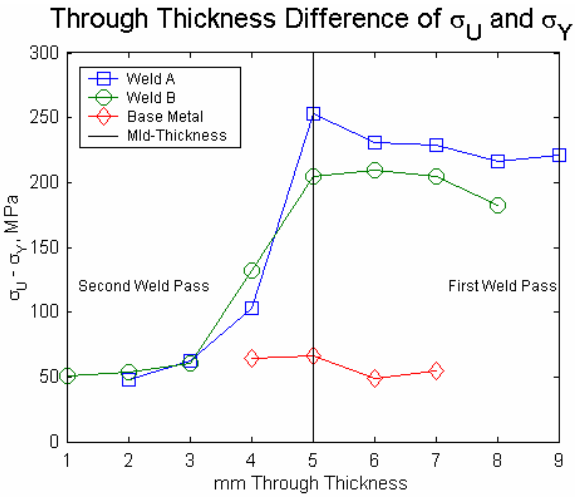

Figure 3-2: Difference of ultimate and yield strengths through the thickness for welds A and B.

The difference between ultimate and yield strengths were plotted against thickness in Figure 3-2 for welds A and B as an indication of the material's ability to strain harden. In the second weld pass, the difference was similar to base metal: about 50 MPa. By mid-thickness however, the difference increased by 205 and 154 MPa for welds A and B, respectively. This represents a 432% and 305% increase for welds A and B, respectively. A large difference between yield and ultimate strength indicates a greater capacity to strain-harden. This removes strain energy available for crack extension. Since J-integral tests include deformation at the crack tip, the increase in the

difference between ultimate and yield strengths from second pass to first was anticipated to affect toughness and crack extension through the weld material thickness. Given these results, higher extensions were anticipated on the second weld pass side than on the first.

3.2 Crack Plane Microhardness

In order to correlate hardness to toughness, the hardness data in Figure 2-2 and Figure 2-3 needed to be reduced to hardness at the crack plane. Three adjacent columns of data approximately centered about each vertical line in Figure 2-3 were removed from the rest of the data set. The three columns were then averaged together for each row to provide an estimate of the hardness of the crack plane through the thickness. This process is illustrated in Figure 3-3 for the advancing side hardened region of weld B.

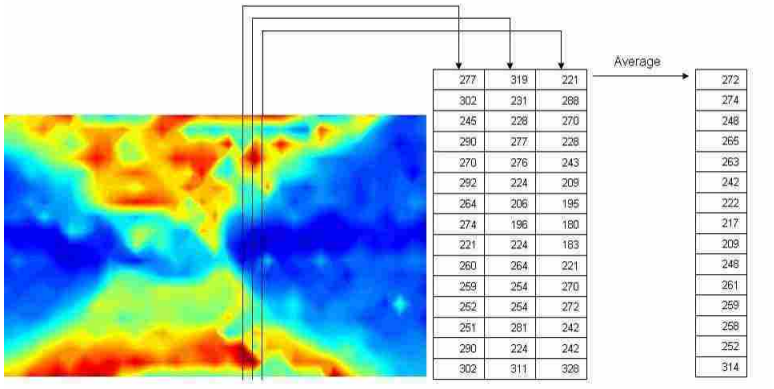

Figure 3-3: Process used to determine average crack plane hardness.

Average hardness was then plotted against thickness for each weld. Additionally, horizontal lines representing the maximum and minimum base metal hardness of 221 and 174 were also plotted for comparison. Since side grooves were implemented, data at the

edges were removed and Figure 3-4 represents the hardness through the reduced thickness at the crack plane.

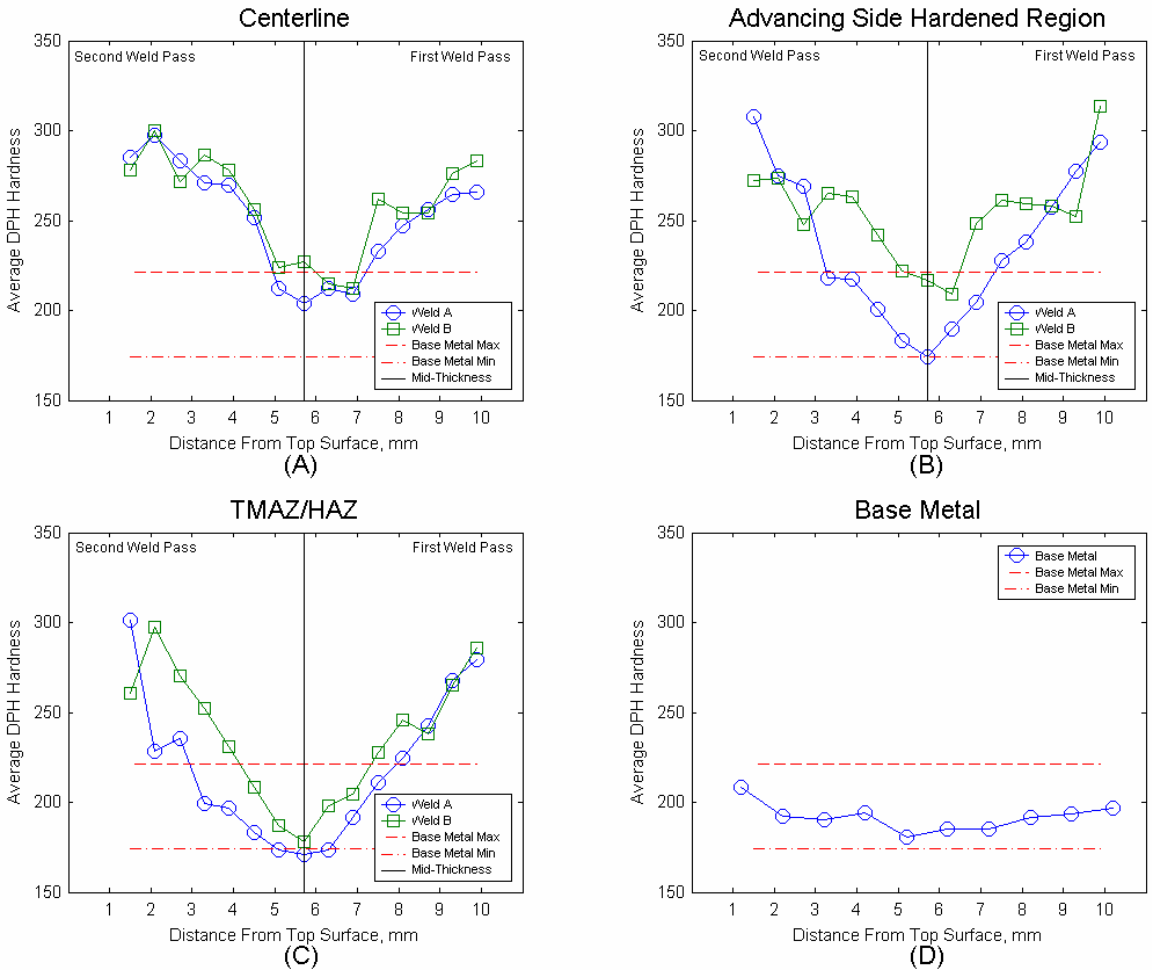

Figure 3-4: Hardness across each crack plane and for weld A and B. (A) centerline, (B) advancing side hardened region, (C) TMAZ/HAZ, and (D) base metal.

Results shown in the through-thickness hardness traces of Figure 3-4 demonstrate similar trends as those seen in through-thickness tensile properties. All crack planes showed minimum hardness at mid-thickness. Additionally, maximum hardness was at the edges of the sample, and correlate to maximum yield and ultimate strengths and

minimum elongations. Centerline hardness traces in Figure 3-4A show an average 10% and 7% decrease in hardness from second weld pass to first for weld A and B respectively. This parallels the yield strength decrease of 11% and 13% for welds A and B respectively.

Figure 3-4 also shows that the welded samples have crack plane hardness similar to the base metal at mid-thickness. The presence of material at mid-thickness with hardness and tensile properties similar to base metal suggests that this location would have higher toughness and would show properties similar to base metal. Conversely, harder and stronger material flanking the mid-thickness region would decrease the ability of the edge material to work harden, leaving more energy available to drive a crack. Crack extensions were therefore anticipated to be higher at the edges than at mid-thickness.

3.3 J-Integral Fracture Toughness

As described in Section 2.5, J integral fracture toughness tests were conducted per both ASTM 1820 and BS 7448. Resistance curves generated from collected J-Δa data were analyzed per ASTM 1820 and BS 7448 to estimate the initiation toughness, J_q. Figure 3-5 lists the qualified initiation toughness values (J_q) for each weld with a corresponding photograph of crack location. Resistance curves used to generate these values are included in Appendix C.

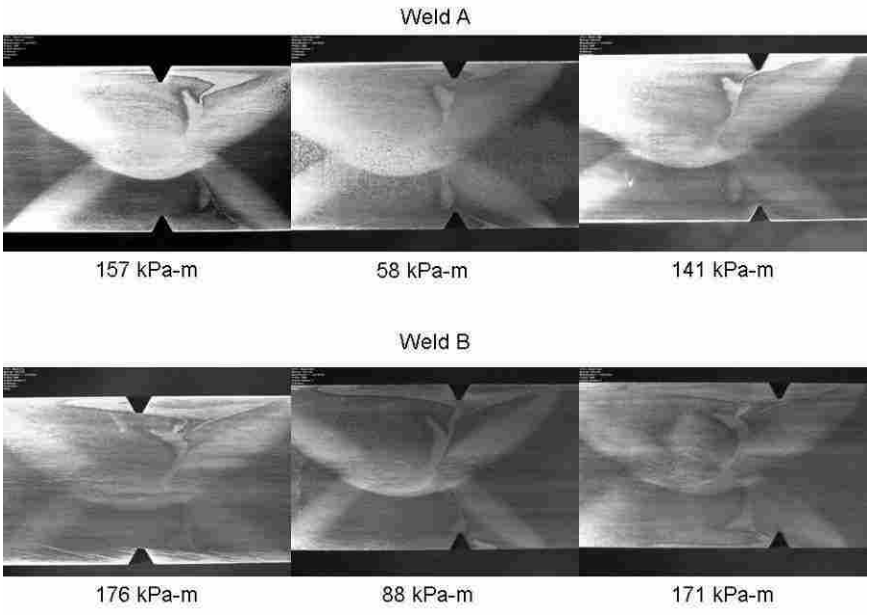

Figure 3-5: Initiation toughness (J_q) and associated crack plane.

The J_q values were then compared to base metal initiation toughness, 235 kPa-m, and presented in Table 3-1 and graphically in Figure 3-6A. These show that friction stir welding resulted in material with lower toughness than base metal. However, increasing the rotational speed from 340 RPM in weld A to 490 RPM in weld B increased toughness on all crack planes.

Table 3-1: Comparison of initiation fracture toughness.

		J_q (kPa-m)	% of Base Metal Toughness	% Increase From Weld A to Weld B
	Base Metal	235	N/A	N/A
Weld A	Centerline	157	66.8%	N/A
	ASHR*	58	24.7%	N/A
	TMAZ/HAZ	141	60.0%	N/A
Weld B	Centerline	176	74.9%	12.2%
	ASHR*	88	37.4%	50.4%
	TMAZ/HAZ	171	72.7%	21.5%

*Advancing Side Hardened Region

To determine if J_q qualifies as the plane strain initiation toughness, $J_{IC,}$ each J_q was used in Equation (3) and compared against the thickness (B) and remaining ligament (b_0). By this procedure J_q qualified as the plane strain initiation toughness for all samples. As such, the plane strain fracture toughness, K_{JIC} (or K_{IC} determined from J_{IC}) was estimated using Equation (4).

$$K_{JIC} = \sqrt{\frac{J_{IC} \cdot E}{(1-\nu^2)}} \quad \textbf{(4)}$$

Where *E* is the modulus of elasticity (assumed to be 207 GPa), and *v* is Poisson's ratio (assumed to be 0.3). K_{JIC} fracture toughness values are presented in Table 3-2 and graphically in Figure 3-6B.

Table 3-2: K_{JIC} Fracture Toughness for Welded Samples.

		K_{JIC} (MPa-$m^{1/2}$)
	Base Metal	232
Weld A	Centerline	189
	ASHR*	115
	TMAZ/HAZ	179
Weld B	Centerline	200
	ASHR*	141
	TMAZ/HAZ	197

*Advancing Side Hardened Region

The increase in toughness from weld A to weld B demonstrates the dependence of fracture properties on weld parameters (see Figure 3-6). The results of Figure 3-1 show an average increase in yield stress for welded samples. Since an increase in yield stress typically reduces toughness, it is little surprise that base metal toughness exceeded weld metal toughness for both sets of parameters. However, tensile and hardness properties

for both welds were similar, yet a significant difference in toughness was measured between weld A and B for all crack planes. Parameters relating to toughness (i.e. thickness, temperature, etc.) were constant for all tests and only the weld RPM was changed. This suggests that the increase in toughness from weld A to B is related to the stirring process, and points to microstructure as a likely difference between welds.

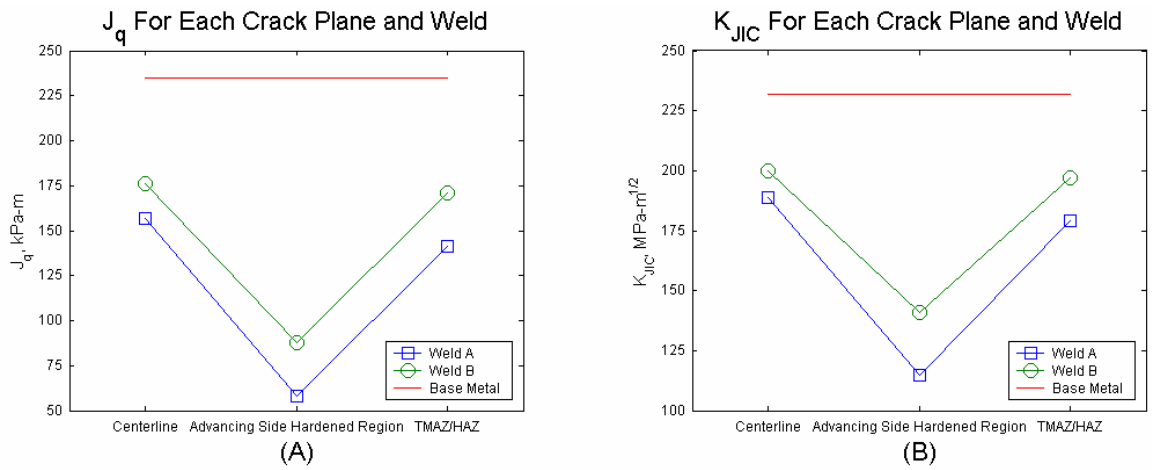

Figure 3-6: Comparison of both the J_q (A) and K_{JIC} (B) toughness parameters for each weld and for each crack plane tested.

J_q, J_{IC}, and K_{JIC} results were subjected to the qualification requirements of both ASTM 1820 and BS 7448 as described in Section 2.5 in order to be further validated. Qualification requirements pertaining to the test equipment, machining tolerances, fixture alignment, test rate, and temperature were all met. Additional qualification requirements applying to the adjustment of J-a data and determination of J_q were also met. However, weld material heterogeneity caused uneven crack fronts and irregular crack extension. Since both standards require straight and uniform crack extensions, qualification of J_q as J_{IC} warrants further scrutiny. Therefore, a thorough discussion of the crack front characteristics and qualification requirements follows.

3.4 Crack Front Characteristics

Figure 3-7 reports the final crack length extensions from the fractured samples that were tested to 100% of the crack extension limit. In accordance with both standards, nine measurements of the initial and final crack length were made at locations equally spaced through the sample thickness. These were then subtracted to produce Δa. The plots in Figure 3-7 compare the crack extension (ordinate) to the nine locations through the thickness (abscissa). Measurements 1 thru 4 then pertain to the second weld pass, measurement 5 is at mid-thickness, and 6 thru 9 correspond to the first weld pass.

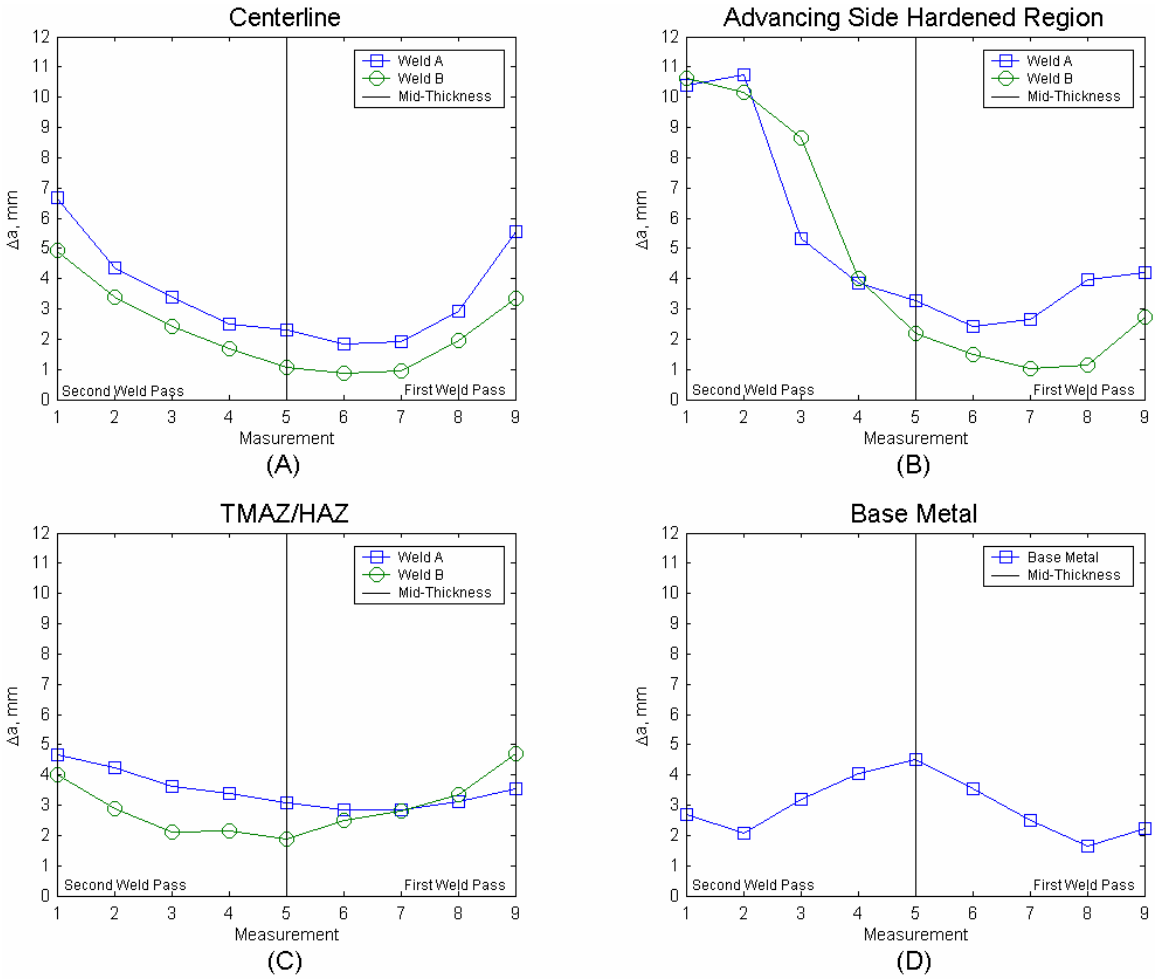

Figure 3-7: Crack extension measurements for samples tested to 100% the crack extension limit. (A) centerline, (B) advancing side hardened region, (C) TMAZ/HAZ, and (D) base metal.

Since the final extent of the crack depended upon termination of the test when a desired maximum crack extension was reached, only tests terminated at similar crack extensions may be compared. Table 3-3 reports the final crack extension reached by the samples presented in Figure 3-7. The base metal, both advancing side hardened region, and the weld A TMAZ/HAZ samples have similar estimated final crack extensions, and may be compared. The weld centerline samples were terminated 0.8 mm apart, and accounts for the difference between the two samples in Figure 3-7A. Figure 3-7; therefore, is presented here as a means to compare the shape of the final crack, and not necessarily the final extent of the crack.

Table 3-3: Test Termination Crack Extension Limits.

		Δa (mm)
	Base Metal	2.92
Weld A	Centerline	2.87
	ASHR*	2.97
	TMAZ/HAZ	2.99
Weld B	Centerline	2.06
	ASHR*	2.95
	TMAZ/HAZ	2.51

*Advancing Side Hardened Region

3.4.1 Crack Front Qualification Requirements

The observed crack fronts of Figure 3-7 were subjected to additional requirements in order to further qualify the J-Δa data reported in Appendix C. Table 3-4 shows how the observed crack fronts fared in relation to the qualification requirements of both ASTM and BS standards. The qualification requirements are categorized across the first row of Table 3-4. The categories where samples tended to fail are the correlation

coefficient for the Data Adjustment, Crack Extension, Final Crack Extension Estimate, and Final Crack Front Straightness.

The Data Adjustment requirement applies a polynomial curve fit to the J-a data (see ASTM 1820, Section A9.3) which provides a sufficient estimate of the initial crack length (a_{0q}) to calculate Δa. J_q is very sensitive to this estimate and the correlation coefficient therefore must be greater than 0.96 However, because it was not known from the beginning when the material would initiate cracking, J-a data from very low loads was collected and included in the curve fit. Calculation of both J and a are very sensitive to load, and the subsequent data at low load levels is scattered, reducing the correlation coefficient. To address this, error from the initial estimate of crack length was assumed mitigated by the abundance of qualified data from three different samples used to estimate of J_q. Also, since no correlation coefficient was below 0.91 and the initial crack length estimates met qualification requirements, relaxation of this requirement seemed justified.

The Crack Extension, Final Crack Extension Estimate, and Final Crack Front Straightness requirements pertain to the final crack lengths, and are briefly described here. The Crack Extension category stipulated that all nine measurements of crack extension were the same within a given percentage. The Final Crack Extension Estimate category relates to how well the final crack extension was estimated by compliance when compared to the physical measurement of extension. The Final Crack Front Straightness category required the final crack length to be straight within a certain percentage.

Table 3-4: Qualification requirements results by standard.

			Data Adjustment			Spacing		Initial Crack Estimate		Initial Crack Front Straightness		Crack Extension		Final Crack Extension Estimate		Final Crack Front Straightness	
			ASTM Only			ASTM	BS	ASTM	BS	ASTM	BS	ASTM	BS	ASTM	BS	ASTM Only	
			A9.3.3.2		A9.4												
		Sample	R > 0.96	More than 3 Points between 0.4JQ and JQ and total # points > 8	abs(a0-aoq)<0.1W	A9.6.4 and A9.6.6.6	12.3	A9.4	10.3.2	9.4.1.1	9.9.2	9.1.5.1	9.9.3	9.1.5.2	10.3.3	9.1.4.2	Final Δa (Estimated)
	Base Metal	2	Fail	Pass	Pass	Pass	Pass	Pass	Pass	Pass	Pass	Pass	Non-Uniform	Pass	Pass	Fail	2.92
		3	Fail	Pass	Pass	Pass		Pass	Pass	Pass	Pass	Fail	Non-Uniform	Pass	Pass	Fail	1.61
		4	Fail	Pass	Pass	Pass		Pass	Pass	Pass	Pass	Fail	Non-Uniform	Fail	Pass	Pass	0.56
Weld A	Centerline	1	Pass	Pass	Pass	Pass	Pass	Pass	Pass	Pass	Pass	Pass	Non-Uniform	Pass	Pass	Fail	2.87
		2	Pass	Pass	Pass	Pass		Pass	Pass	Pass	Pass	Fail	Non-Uniform	Pass	Pass	Fail	1.54
		4	Pass	Pass	Pass	Pass		Pass	Pass	Pass	Pass	Fail	Non-Uniform	Fail	Fail	Fail	1.37
	Advancing Side Hardened Region	2	Pass	Pass	Pass	Pass	Pass	Pass	Pass	Pass	Pass	Fail	Non-Uniform	Fail	Fail	Fail	2.97
		3	Pass	Pass	Pass	Pass		Pass	Pass	Pass	Pass	Fail	Non-Uniform	Pass	Pass	Fail	1.41
		4	Pass	Pass	Pass	Pass		Pass	Pass	Pass	Pass	Fail	Non-Uniform	Pass	Pass	Fail	0.53
	TMAZ/HAZ	1	Fail	Pass	Pass	Pass	Pass	Pass	Pass	Pass	Pass	N/A	Non-Uniform	N/A	N/A	N/A	1.80
		2	Pass	Pass	Pass	Pass		Pass	Pass	Pass	Pass	Pass	Non-Uniform	Pass	Pass	Pass	2.99
		3	Pass	Pass	Pass	Pass		Pass	Pass	Pass	Pass	Fail	Non-Uniform	Fail	Fail	Fail	0.58
Weld B	Centerline	3	Fail	Pass	Pass	Pass	Pass	Pass	Pass	Pass	Pass	Fail	Non-Uniform	Pass	Pass	Pass	0.45
		5	Pass	Pass	Pass	Pass		Pass	Pass	Pass	Pass	Fail	Non-Uniform	Pass	Pass	Fail	2.14
		6	Pass	Pass	Pass	Pass		Pass	Pass	Pass	Pass	Fail	Non-Uniform	Pass	Pass	Fail	2.06
	Advancing Side Hardened Region	1	Pass	Pass	Pass	Pass	Pass	Pass	Pass	Pass	Pass	Fail	Non-Uniform	Fail	Fail	Fail	2.94
		2	Fail	Pass	Pass	Pass		Pass	Pass	Pass	Pass	Fail	Non-Uniform	Fail	Fail	Fail	2.95
		4	Fail	Pass	Pass	Pass		Pass	Pass	Pass	Pass	Fail	Non-Uniform	Fail	Fail	Fail	0.78
	TMAZ/HAZ	0	Pass	Pass	Pass	Pass	Pass	Pass	Pass	Pass	Pass	N/A	Non-Uniform	N/A	N/A	N/A	2.90
		2	Fail	Pass	Pass	Pass		Pass	Pass	Pass	Pass	Pass	Non-Uniform	Pass	Pass	Pass	1.62
		3	Pass	Pass	Pass	Pass		Pass	Pass	Pass	Pass	Fail	Non-Uniform	Fail	Fail	Pass	0.55

Figure 3-7 shows why the samples failed requirements in these categories: crack extensions were highly irregular and non-uniform. Crack front irregularity is most likely due to a number of competing factors and necessitates further analysis and discussion.

3.4.2 Base Metal Samples

Figure 3-8A shows the base metal sample that was terminated at maximum crack extension. Crack fronts were cusped with higher extensions at mid-thickness (Figure 3-7D). The base metal sample terminated between 0.1 mm and 0.3 mm crack extension exhibited the same characteristic. Examination of the microhardness map (Figure 3-8B) revealed only slight variation in hardness through the thickness of the sample (maximum = 221, minimum = 174, average = 193). Figure 3-8B shows that a majority of the softer material is located at mid-thickness and is flanked by harder material at the edges. It would follow then that lower extensions would be observed at mid-thickness where hardness is lower. But since the opposite was true, other factors were at work.

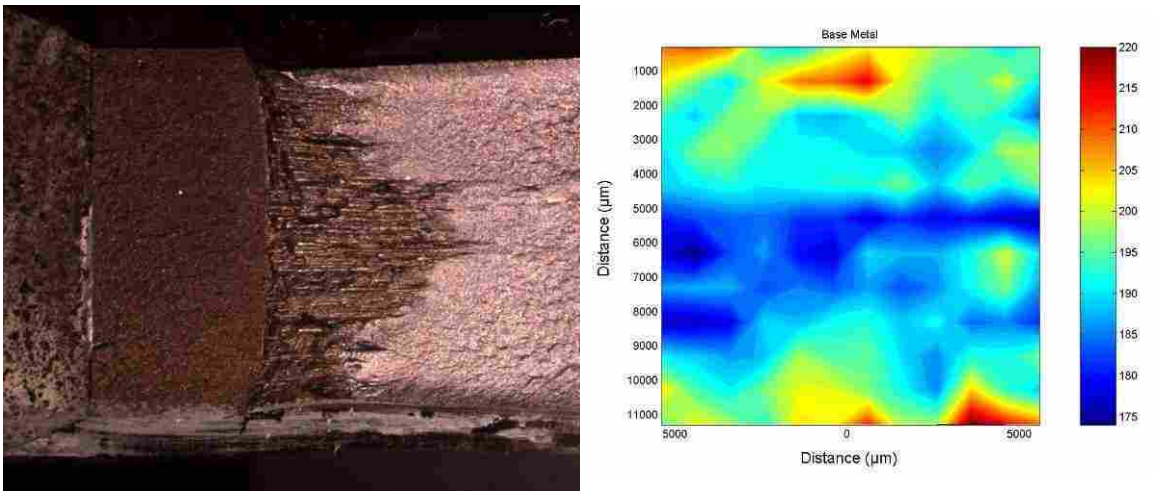

(A) (B)

Figure 3-8: (A) base metal fracture surface. (B) base metal hardness map.

The stress-strain condition affects the appearance of the crack front. Because the qualification requirements of both ASTM 1820 and BS 7448 were not met, the plane strain condition determined by Equation (3) warrants scrutiny. To determine the stress-strain condition at the crack tip, the following method was utilized. Since this analysis applies equally to the welded samples, they are included here with the analysis of the base metal samples for discussion later.

In order to resolve differences between crack planes that the tensile data in Figure 3-1 does not provide, the through thickness Vickers hardness measurements reported in Figure 3-4 and strain hardening coefficients estimated from tensile tests were used to estimate yield stress (Appendix D). The hardness based estimate of yield stress was then combined with the estimated K_{JIC} (Table 3-2) to calculate the plane stress plastic zone radius in Equation (5). Theta (θ) was set equal to zero, limiting the analysis to the crack plane.

$$r_y = \frac{K^2}{2\pi\sigma_{ys}^2}\cos^2\frac{\theta}{2}\left(1+3\sin^2\frac{\theta}{2}\right) \quad \textbf{(5)}$$

The calculated radii were then divided by sample thickness. By calculating the ratio in this manner, it can be determined whether or not sufficient material existed in the thickness direction to cause the plane stress condition at the edges to transition to plane strain at mid-thickness. Generally, if the sample thickness is less than or equal to the plane stress plastic zone radius, a plane stress condition can be assumed through the thickness. Also, sufficient material exists to induce plane strain conditions when the thickness is ten times the plane stress plastic zone radius [13]. Therefore, ratios greater than one were assumed to indicate plane stress conditions, while ratios less than 0.1 were assumed to indicate a plane strain condition. These results are presented in Figure 3-9.

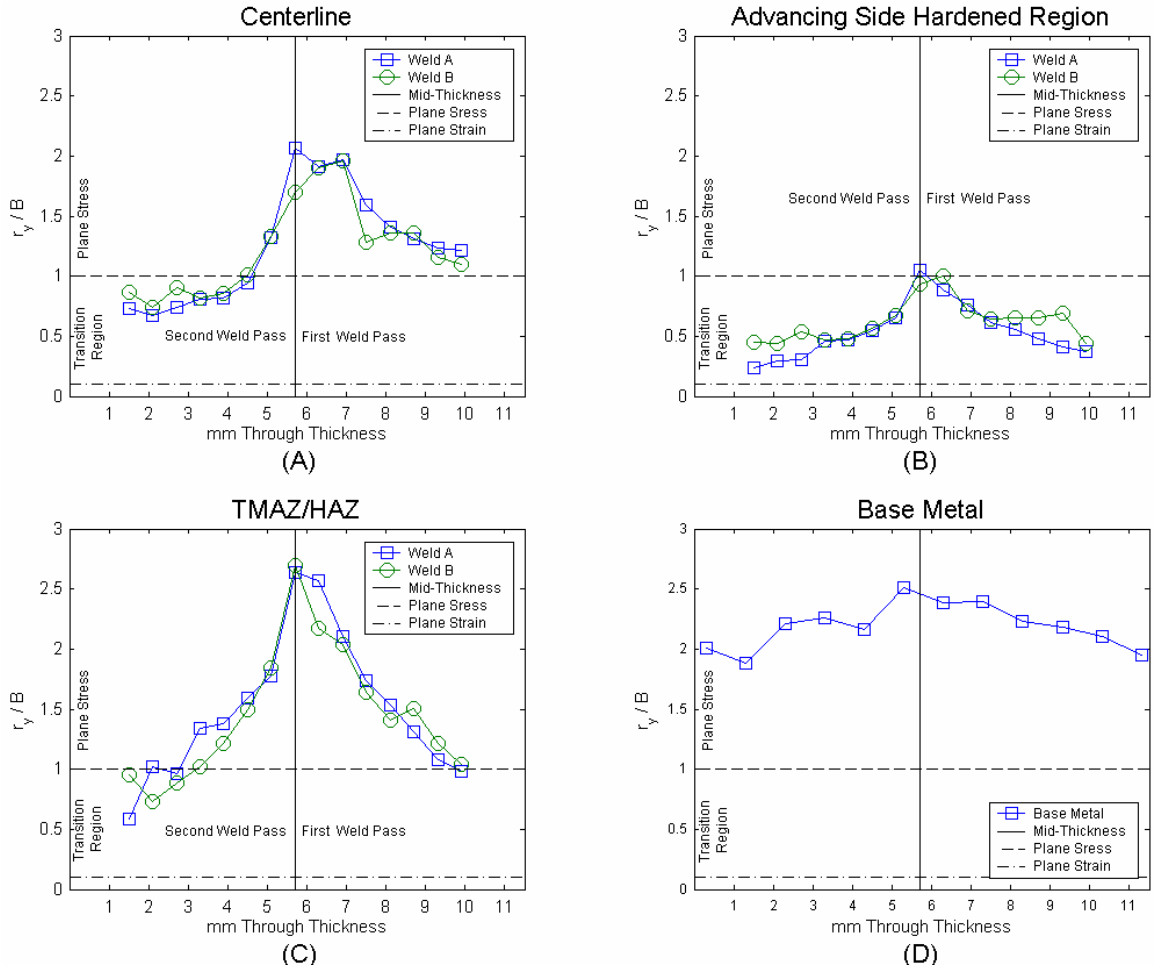

Figure 3-9: Ratios of plastic zone radius to thickness plotted against the through thickness dimension for each weld and (A) centerline, (B) advancing side hardened region, (C) TMAZ/HAZ , and (D) base metal samples.

The stress-strain condition determined by these ratios is limited. For example, Figure 3-9A shows ratios near 0.75 at the surface of the second weld pass for both samples, indicating a mixed mode plane stress-plane strain condition. But since it is at the free edge of the sample, a plane stress condition is known to exist. Therefore, the ratio of 0.75 does not describe the stress-strain condition at this particular location near the edge. Rather, it describes the stress-strain condition of a theoretically homogeneous sample that has the same yield strength as this location, and has the same thickness used

to calculate the ratio. In other words, since only a discrete yield strength from a specific location within the thickness was used to calculate r_y, and therefore r_y/B, the ratio describes the stress-strain condition as if the entire thickness had that particular yield strength.

Despite this limitation, this analysis still proved useful. For a homogeneous sample, a ratio greater than one means that plane stress conditions exist everywhere through the thickness. Similarly, a ratio greater than one at a discrete location implies the sample had insufficient thickness to reduce the plastic zone size associated with that particular yield strength, resulting in plane stress conditions. Therefore, a ratio greater than one equates to plane stress, regardless of the location within the thickness where the yield strength was measured. Additionally, since these ratios infer how much thickness is required to reduce the plane stress condition at each edge to a plane strain condition at mid-thickness, ratios located near mid-thickness are representative of the stress-strain condition unlike ratios calculated at the edges.

It is apparent from Figure 3-9D that plane stress conditions dominated in the base metal samples, and the observed crack fronts in the base metal samples were primarily a result of this condition. A plane stress condition causes the fracture plane to align itself to planes at 45° angles to the thickness and loading directions. This produces a shear type failure, and associated shear lips. In typical materials, a cusped crack front results as the flat fatigue precrack transitions to 45° planes. The cusp terminates when shear lips converge with each other at mid-thickness.

Observed shear lips were much smaller than the thickness dimension; however, and did not converge at mid-thickness. Smaller shear lips are expected in ferritic steels

like HSLA-65, and measured approximately 0.75 mm wide. Nonetheless, the plane stress condition of these samples still forced the crack plane to transition to 45° planes, and the observed cusped crack front was produced as evidence of a plane stress condition.

3.4.3 Weld Centerline Samples

The weld centerline samples exhibited non-uniform crack growth (Figure 3-7A). Higher final crack lengths were measured on the second weld pass compared to the first weld pass (Figure 3-7A) for both weld A and B. This trend is the same as those observed for yield and ultimate tensile strengths (Figure 3-1A and B) and the crack plane hardness (Figure 3-4A).

The observed crack front was a result of plane stress conditions at the crack tip and variation in the through thickness yield strength. Figure 3-9A shows that a lower yield strength at mid-thickness produced material that is in plane stress, resulting in increased toughness which reduced crack extensions. Figure 3-9A also shows that the reduction of yield strength due to overlapping weld passes increased the plastic zone radius between weld passes for both weld A and B, increasing toughness and reducing extensions. Noting the limitations described previously for Figure 3-9, the free edges of the sample must have been in plane stress; but due to increased yield strength at the edges, the plastic zone was smaller, toughness was reduced, and extensions were higher.

Additional evidence of the change in stress-strain behavior through the thickness of the centerline samples is shown in Figure 3-10. SEM analysis of the fracture surface revealed an increase in deformation dimple size from the second weld pass (20 to 50 microns) to the first (20 to 80 microns). These results correlate with lower yield stress, higher plasticity, higher toughness, and lower extensions in the first weld pass.

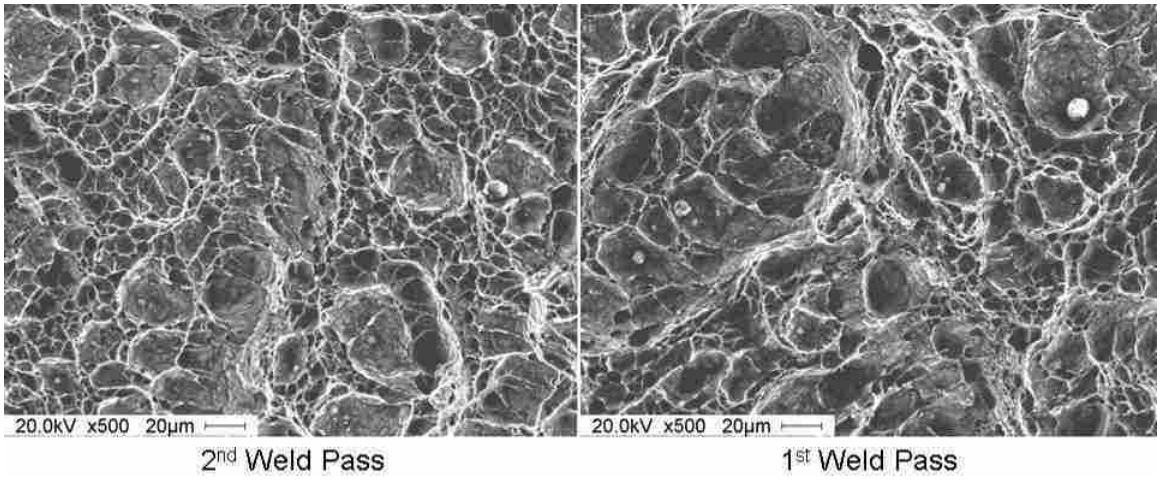

Figure 3-10: Weld centerline fractographs comparing deformation dimples of weld passes (500x).

3.4.4 Advancing Side Hardened Region Samples

The advancing side hardened region proved to be the region of lowest toughness. These samples showed irregular and uneven crack extensions, but to a much greater degree than other samples. Second weld pass crack extensions exceeded first pass extensions by about 7 mm, the largest difference observed in this study (Figure 3-8B). This is equivalent to a 250% increase over first weld pass crack extensions. Additionally, the location of highest extension corresponded with the location of highest hardness on microhardness maps (Figure 2-2) and the stir zone-TMAZ interface at the root of the pin in the second weld pass.

The relationship between the observed crack front appearance and tensile properties was not as obvious as the centerline samples. Figure 3-11 presents the through thickness difference of ultimate and yield strengths (A) next to the plot of final crack extension (B). Comparison of these figures showed low crack extensions where the difference was high, and vice-versa. Plotting crack extensions against the difference in ultimate and yield strengths verified an inverse relationship (Figure 3-11C and D).

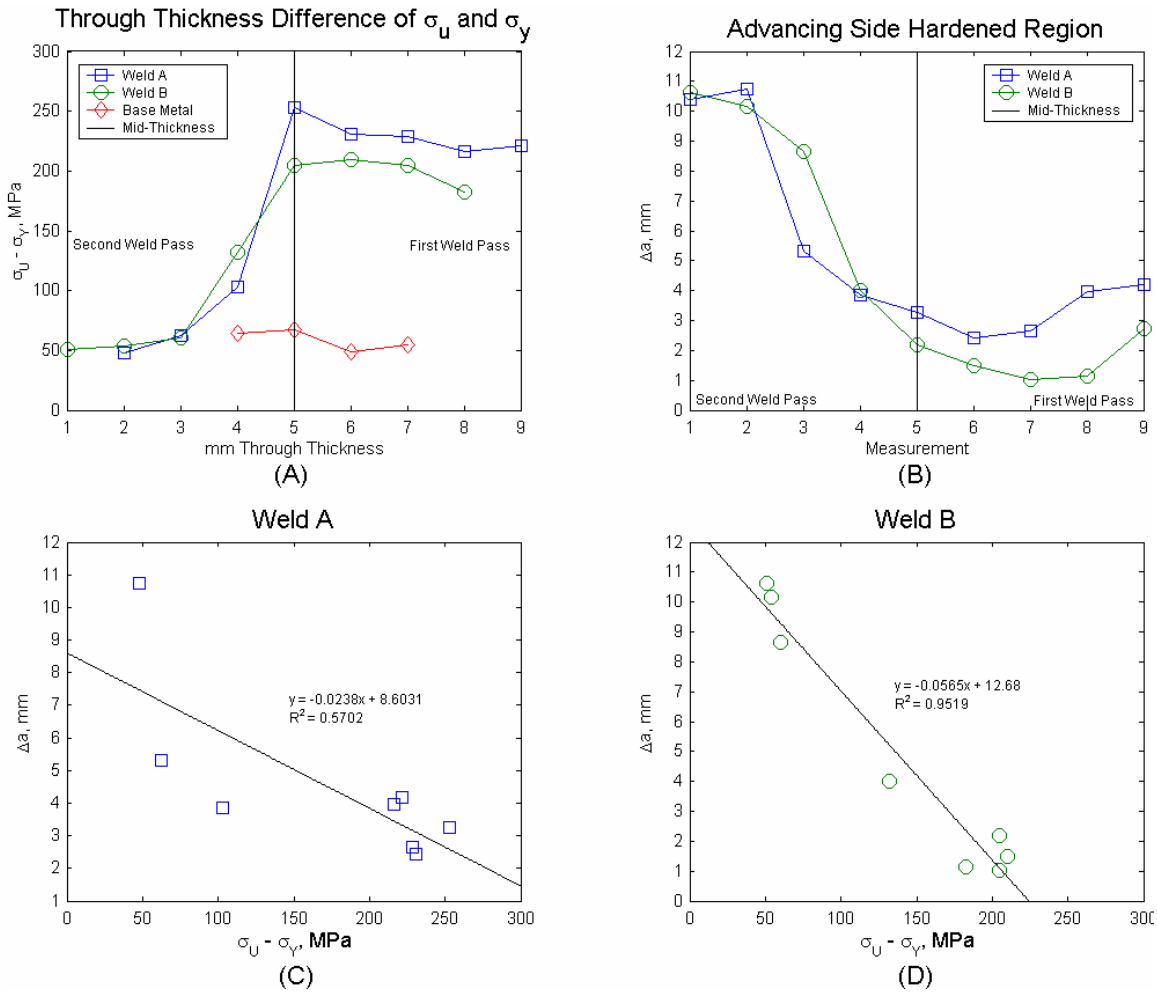

Figure 3-11: Comparison of Figure 3-2A and Figure 3-7B. Plots comparing difference in ultimate and yield strength vs. final crack extension for weld A (C) and weld B (D).

This relationship gives insight to the cracking mechanism and how it was different from other samples. Figure 3-9B and Equation (5) show that high yield strengths reduced plastic zone size. Additionally, the small difference in ultimate and yield strengths in the second weld pass (Figure 3-11A) implies that as the local stresses within the plastic zone increased, the ultimate strength was quickly reached, and crack extension occurred. This combination of reduced plastic zone size and small difference

in ultimate and yield strengths indicates reduced fracture toughness, resulting in increased crack extensions.

Conversely, on the first weld pass, a reduction of yield strength was obtained by overlapping weld passes while maintaining a nearly constant ultimate strength. This increased the difference in ultimate and yield strength nearly five fold. When the sample was loaded, high local stresses ahead of the crack exceeded the yield stress, but the first weld pass was able to develop a larger plastic zone and had more ability to strain-harden. Therefore, strain energy that was available to drive the crack on the second weld pass side was removed by strain hardening on the first weld pass side. A larger plastic zone and greater ability to strain harden delayed failure, increased toughness, and reduced crack extension. Thus the observed crack front was produced: much higher crack extensions on the second weld pass side than on the first.

Despite having similar through thickness properties, the final crack length shapes were quite different for the weld centerline and advancing side hardened region samples. The centerline and advancing side hardened region samples had similar through thickness microhardness traces (Figure 3-4) and shared nearly the same through thickness tensile properties. Yet the centerline samples had crack fronts that paralleled the through thickness yield stress and the advancing side hardened region samples showed an inverse relationship to the ability to strain harden. The reason for this behavior is related to the stress-strain condition of the crack tip. The advancing side hardened region samples showed a mixed mode stress-strain behavior (Figure 3-9B) which differed from the plane stress behavior demonstrated by the centerline samples.

The transition from plane stress could only have occurred as a result of only a few factors. Typically, transition from plane stress to plane strain can be brought on by a reduction in temperature, an increase in sample thickness, or by a detrimental thermo-mechanical process. These methods all act to limit plastic strain within the plastic zone. However, the test temperature and specimen thickness remained constant for all samples. Therefore, the mixed mode stress-strain condition observed in the advancing side hardened region samples is attributable to the thermo-mechanical process of friction stir welding and its effect on the material at this location.

Like the centerline samples, the relative amounts of crack tip deformation exhibited by the second weld pass compared to the first were confirmed by SEM analysis. Figure 3-12 shows SEM fractographs of the advancing side hardened region fracture surface. Analysis of these samples showed a decrease in deformation dimple size from first to second pass. Dimple sizes ranged from 1 to 2 microns on the second weld pass side, and 2 to 5 microns in the first. In fact, these were the smallest deformation dimples of all samples. The small size of these dimples strongly suggests limited plastic deformation and the mixed stress-strain behavior in the advancing side hardened region samples.

The weld B advancing side hardened region samples were also the only samples to demonstrate any instability in crack extension. The unstable crack growth was arrested, did not cause failure of the sample, and testing continued until a final crack extension was reached. It is noted here that the unstable crack growth occurred after stable crack growth per ASTM and BS standards, and therefore, the initiation toughness calculated for the weld B advancing side hardened region samples is still valid. However, an additional

value, J_u was calculated for these samples. J_u represents the value of J at which instability is likely to occur after the onset of stable tearing. For the weld B advancing side hardened region samples, this value is 104 kPa-m.

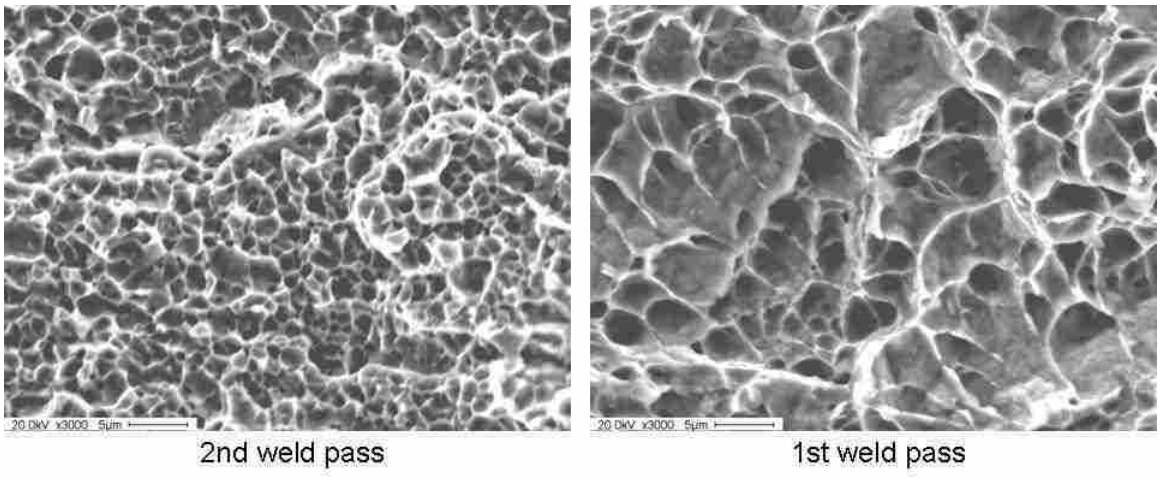

Figure 3-12: Comparison of first and second weld pass deformation dimples for the advancing side hardened region samples (3000x).

3.4.5 TMAZ/HAZ Samples

TMAZ/HAZ crack extensions were non-uniform, but the final crack front was nearly straight (Figure 3-7C and Table 3-4). As shown in Figure 3-13, a slight curvature of the initial fatigue precrack existed, but each measurement was within 10% and 20% of the average and considered straight by both ASTM and BS standards, respectively. The final crack front was also straight. However, crack extensions (or the difference between final and initial crack lengths) were higher at the edges than at mid-thickness, and varied through the thickness enough to be considered non-uniform. Hence, straight initial and final crack fronts were reported, in addition to non-uniform extension. Similar to the

advancing side hardened region, this result also stemmed from through thickness tensile properties and the stress-strain condition of the crack tip.

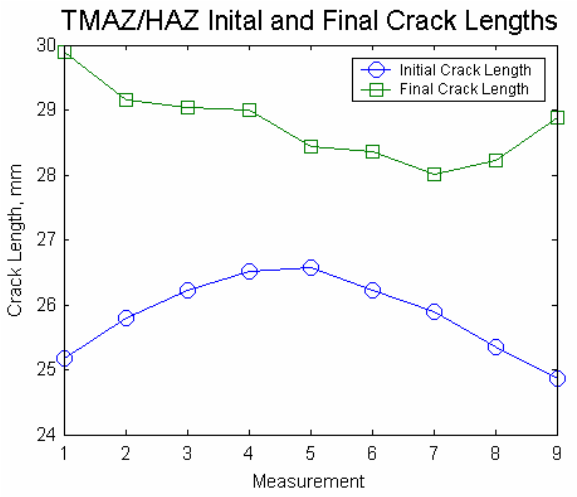

Figure 3-13: TMAZ/HAZ initial and final crack length measurements.

The mid-thickness yield stress and hardness of the TMAZ/HAZ samples were at or below the base metal minimum (Figure 3-1A and Figure 3-4C). This resulted in plane stress conditions prevailing at mid-thickness in these samples (Figure 3-9C). Figure 3-9C also shows that the TMAZ/HAZ samples had ratios greater than one through most of the thickness, and were the highest for the welded samples. Given that edge interaction is not accounted for in Figure 3-9C, the crack front was likely in plane stress through the entire thickness. Despite having plane stress conditions similar to the base metal and centerline samples, the crack front appeared much different than these other samples.

At mid-thickness, the TMAZ/HAZ samples functioned more like the base metal samples. Mid-thickness crack extensions were driven by the tendency of a material to transition from the crack plane to 45° planes in plane stress. However, unlike the base

metal samples, the TMAZ/HAZ samples increased in yield strength and hardness towards the edges, much like the centerline samples, (Figure 3-1A and Figure 3-4C). This reduced the plastic zone size and the local toughness, increasing crack extensions at the edges. Hence, high extensions at the edges equaled the mid-thickness crack extensions as a result of material heterogeneity; causing non-uniform extensions but a straight final crack front.

For the TMAZ/HAZ samples, the plane stress cracking mechanism at mid-thickness is confirmed in the fractograph of Figure 3-14. The fatigue precrack is labeled on the left. To the right, tears that run parallel the crack direction are indicated with arrows; the top tear being located at mid-thickness. The two edges of the tears each open to a 45° angle, which suggest a local shear-type failure. This gives evidence to the plane stress condition prevalent during fracture [13]. The sample edges (not shown) exhibited features similar to the weld centerline samples: deformation dimples of similar size, and increased in size from second weld pass to first. Similarities to centerline samples at the edges confirm the limited deformation which increased crack extensions at the edges.

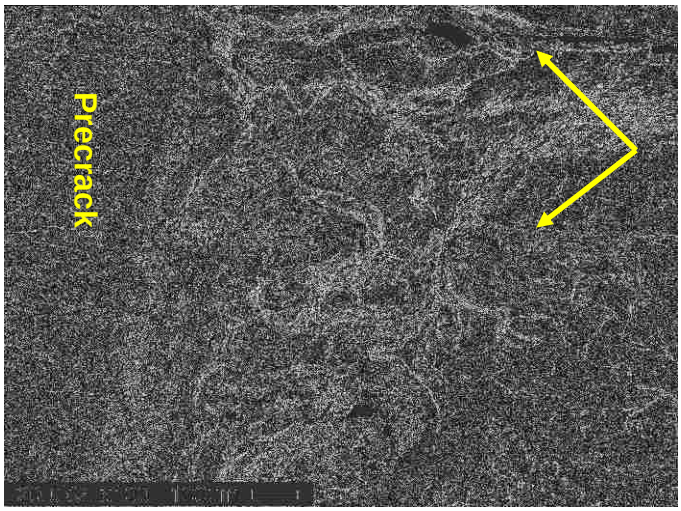

Figure 3-14: Fractograph of TMAZ/HAZ sample at mid-thickness (100x).

3.5 Microstructure

As a supplement to the crack front characteristics of the previous section, the microstructure was examined. This was done in order to explain the observed crack front phenomena and to briefly describe how weld parameters affected the microstructure, and thereby, toughness. Relative weld microstructures were compared by taking images at fixed distances from the plate surface toward mid-thickness for each weld pass. This analysis was conducted for both welds A and B, and for each crack plane.

Comparison of first and second weld passes revealed evidence of tempering. Figure 3-15 presents images taken from the weld centerline, and shows upper bainite present in both weld passes. In the first weld pass however, coarsening of the bainite structure has occurred. Coalescence of ferrite and cementite phases is also observed. These changes in microstructure indicate that sufficient heat was applied during the second weld pass to cause tempering, reduce the yield strength (Figure 3-1A), increase elongation (Figure 3-1C), increase toughness, and reduce crack extensions (Figure 3-7). Although not shown, tempering was observed for both welds and for all crack planes.

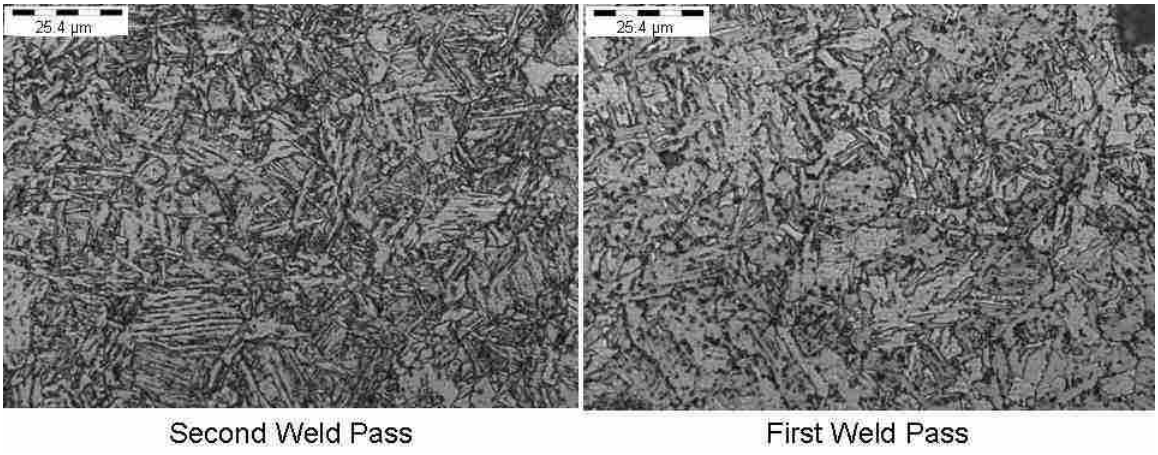

Figure 3-15: Microstructural comparison of weld passes showing evidence of tempering (1000x).

Increasing the rotational speed affected the microstructure and accounts for the increase in toughness between weld A and B centerline samples. The micrographs in Figure 3-16 show the centerline microstructure for welds A and B. Since both welds were conducted at the same heat input, it is no surprise the microstructure appears very similar. This necessitated a more detailed analysis to characterize differences between welds. Therefore, lath width of the bainite structure for each weld was estimated using a linear intercept method [14], and the results are presented in Table 3-5.

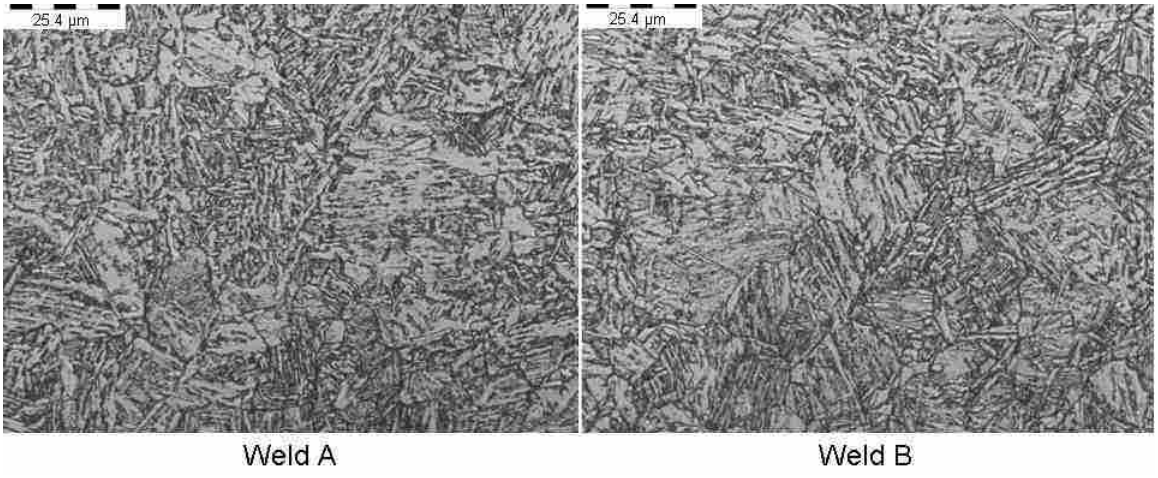

Figure 3-16: Comparison of weld A and B microstructures (1000x).

Table 3-5: Lath width measurement results.

	Average Lath Width	95% Confidence Interval	Relative Accuracy
	µm	µm	%
Weld A	1.37	0.12	8.5
Weld B	1.19	0.11	9.4

Lath width decreased 13% from 1.37 µm to 1.19 µm by increasing the rotational speed from weld A to weld B. The decrease in lath width from weld A to weld B

suggests that the formation of the ferrite and cementite phases from austenite was affected by rotational speed, as this is the only difference between welds. By increasing the rotational speed, different amounts of work were performed on the material by the friction stir welding process. By changing the amount of work, the recrystallization temperature was affected, resulting in a finer lath width for weld B and increased toughness relative to weld A.

In the advancing side hardened region samples, friction stir welding caused the formation of Widmanstatten ferrite which led to the low toughness observed on this crack plane (Figure 3-17). High heat and high strains due to a combination of tool rotation and forging force limited austenitic grain growth. Additionally, rapid cooling limited diffusion and produced fine ferrite laths. This microstructure increased local yield stresses and severely limited plastic strain, reducing toughness.

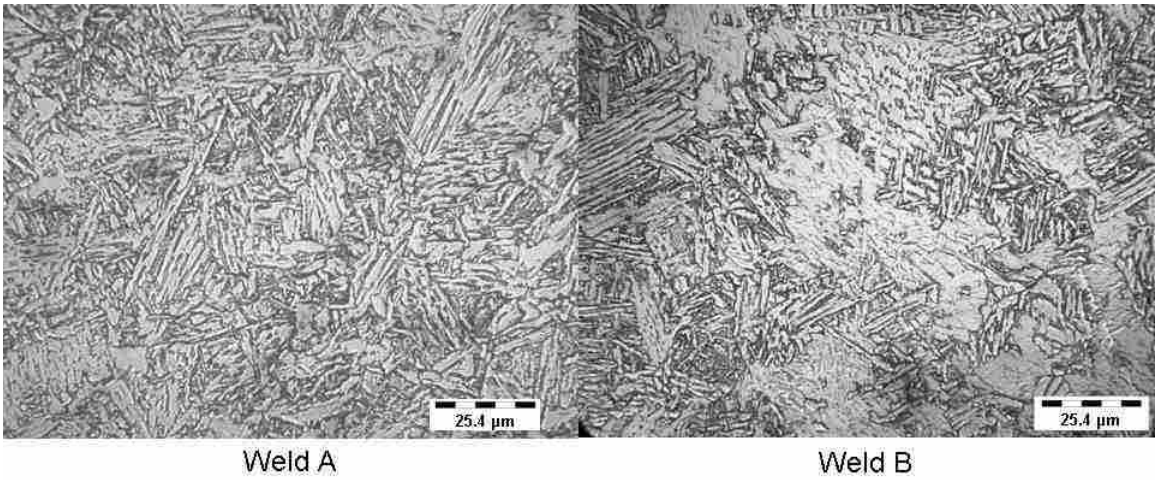

Figure 3-17: Micrograph showing Widmanstatten microstructure in the advancing side hardened region samples for weld A and B (1000x).

Widmanstatten ferrite was isolated within a banded region within the advancing side hardened region samples. These regions are highlighted in Figure 3-18 for weld A and B: weld A is wedge shaped and weld B is 'y' shaped. The change in shape is a result of increasing the weld rotational speed. While not directly on the crack plane, the ductile centerline-like material between the two forks of Widmanstatten ferrite in weld B was still within the plastic zone. This likely increased toughness due to decreased amounts of Widmanstatten ferrite within the plastic zone when compared to weld A, but also led to the instability seen in these samples. Toughness in the advancing side hardened region is therefore related to the formation of Widmanstatten ferrite as a result of rotational speed. Furthermore, since the crack plane was placed to specifically sample the hardened region near the root of the pin and not Widmanstatten ferrite, different amounts of Widmannstatten were subsequently sampled and could have contributed to the differences in toughness observed on this crack plane.

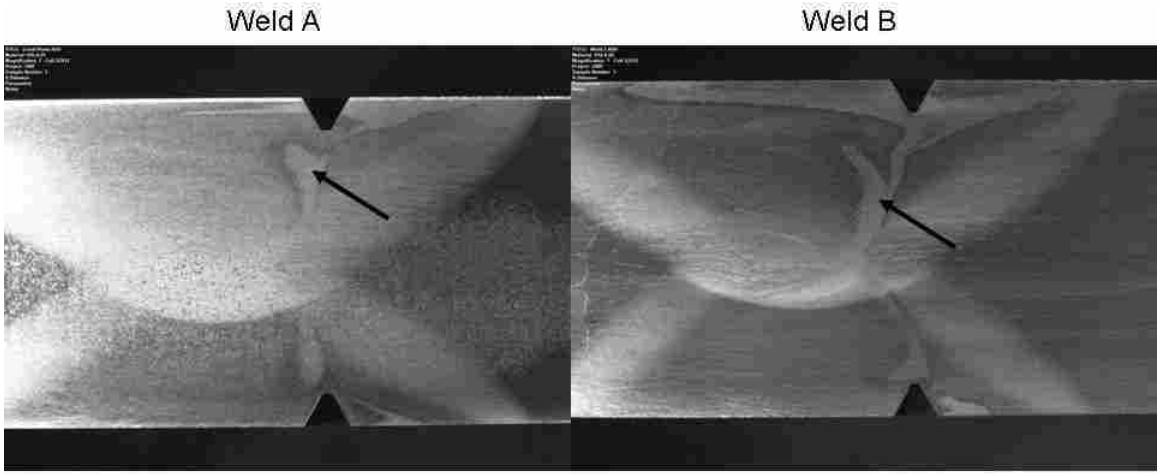

Figure 3-18: Macrographs illustrating differences in the shape of the banded region for both weld A and B.

4 Conclusions

Using current ASTM 1820 and BS 7448 standards, mode one elastic-plastic fracture toughness at room temperature was determined for friction stir processed HSLA-65 in each of three weld planes: the weld centerline, advancing side hardened region, and TMAZ/HAZ. Additionally, toughness of each position was evaluated at two rotational speeds (340 RPM and 490 RPM) and compared with un-welded parent material. Toughness values for all samples failed to meet qualification requirements of both ASTM 1820 and BS 7448 due to insufficient thickness and non-uniform crack extension. Therefore, all fracture toughness values reported were thickness dependent, J_q.

1) Welded samples exhibited lower toughness than the parent material for all crack plane locations for both rotational speeds.
2) The centerline location exhibited the highest weld toughness. Reduction in toughness at the centerline was 33% and 25% less than parent material for welds produced at 340 RPM and 490 RPM, respectively.
3) The advancing side hardened region exhibited the lowest toughness. Toughness on this crack plane was 75% and 63% less than parent material for welds produced at 340 RPM and 490 RPM, respectively.
4) TMAZ/HAZ toughness was 40% and 27% below parent material for welds produced at 340 RPM and 490 RPM, respectively.

5) By increasing the rotational speed to 490 RPM, weld toughness increased relative to welds produced at 340 RPM.
6) Increased weld toughness from 340 RPM to 490 RPM was attributed to microstructural differences as a result of increased rotational speed.
7) Weld tempering caused lower crack extensions in the first weld pass relative to the second in all crack planes and welds.
8) The ASHR samples exhibited the highest crack extensions. In this location, the weld microstructure consisted of Widmanstatten ferrite, a microstructure known to be detrimental to toughness.

5 Recommendations for Future Work

1) While friction stir welding produced material with lower toughness than the base metal material, it is suggested that further study be conducted to explore the parameter window and the relationship of parameters to microstructure and/or toughness to find optimal parameters in regard to toughness.
2) Since plane stress fracture toughness values were obtained in welded material at room temperature, it is recommended that further work be done to explore the role of temperature on fracture toughness of friction stir welds.
3) Refined methods for testing specific regions of microstructure other than ‘weld positional’ are available and could be utilized to measure more specific regions of the weld.
4) Due to the low toughness of the hardened region, thinner samples could be used to specifically test this region, allowing for straighter final crack extensions; thus conforming to qualification requirements.
5) The relationship between weld parameters and the amount of Widmanstatten ferrite produced should be explored.

6 References

1. "Can welding put an end to the airframe rivet?" Aluminum Today, vol. 10, No. 5, 1998, pp. 48-60.

2. Sorensen, C.D., T.W. Nelson, and S.M. Packer, "Tool Material Testing for FSW of High Temperature Alloys," *Proceedings of the 3rd International Symposium on Friction Stir Welding*, 27-28 September 2001, Kobe, Japan.

3. Montemarano, T.W., B. P. Sack, J. P. Gudas, M. G. Vassilaros, and H. H. Vanderveldt, "High Strength Low Alloy Steels in Naval Construction," *Journal of Shipbuilding,* vol 2, No. 3. August, 1986, pp. 145-162.

4. ASTM Standard E1820-01, "Standard Test Method for Measurement of Fracture Toughness," *Annual Book of ASTM Standards,* vol. 3.01, ASTM 1916 Race Street, Philadelphia, PA, 2001.

5. British Standard 7448 "Fracture Mechanics Toughness Tests-Parts 1-4," *British Standards Institution,* 389 Chiswick High Road, London.

6. Fairchild, D. P., "Fracture Toughness Testing of Weld Heat-Affected Zones in Structural Steel," *Fatigue and Fracture Testing of Weldments, ASTM STP 1058,* H. I. McHenry and J. M. Potter, Eds., American Society for Testing and Materials, Philadelphia, 1990, pp. 117-141.

7. Jata, K. V., K. K. Sankaran, J. J. Ruschau, "Friction Stir Welding Effects on Microstructure and Fatigue of Aluminum Alloy 7050-T7451," *Metallurgical and Materials Transactions A,* vol. 31A, no. 9; September, 2000, pp. 2181-2192.

8. Sutton, Michael A., Anthony P. Reynolds, Bangcheng Yang, Robert Taylor, "Mode I Fracture and Microstructure for 2024-T3 Friction Stir Welds," *Materials Science and Engineering A,* vol. 354, 2003, pp. 6-16.

9. Feng, Zhili, Russell Steel, Scott Packer and Stan A. David, "Friction Stir Welding of API Grade X65 Steel Pipes", Oak Ridge National Labs. April, 2005.

10. Konkol, Paul J, James A. Mathers, Richard Johnson, and Joseph R. Pickens, "Friction Stir Welding of HSLA-65 Steel for Shipbuilding," Journal *of Shipbuilding,* vol. 19, 2003 pp. 159-164.

11. Pew, Jefferson Willis, “A Torque Based Weld Power Model for Friction Stir Welding” Thesis. Brigham Young University 2006.

12. Dieter, George E. “Mechanical Metallurgy – Third Edition.” McGraw Hill, ISBN 0-07-016893-8.

13. Hertzberg, Richard W. “Deformation and Fracture Mechanics of Engineering Materials – Fourth Edition.” New Jersey: Hoboken, 1996.

14. ASTM Standard E112-96 (2004)$^{\varepsilon 2}$, “Standard Test Methods for Determining Average Grain Size.” ,” *Annual Book of ASTM Standards,* vol. 3.01, ASTM 1916 Race Street, Philadelphia, PA, 2006.

Appendix A. Tool Details

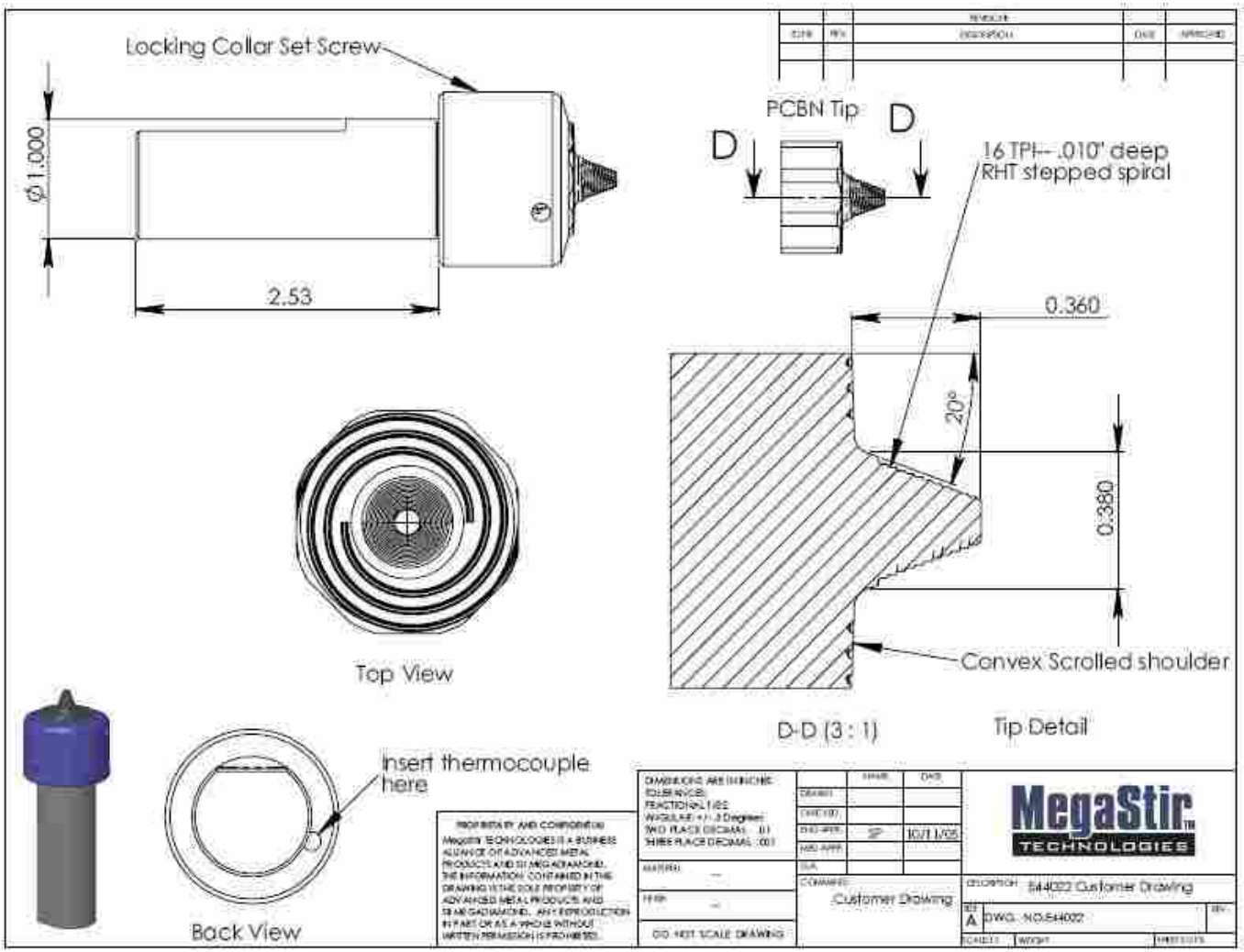

Figure A-1: Weld tool details.

Appendix B. Specimen Details

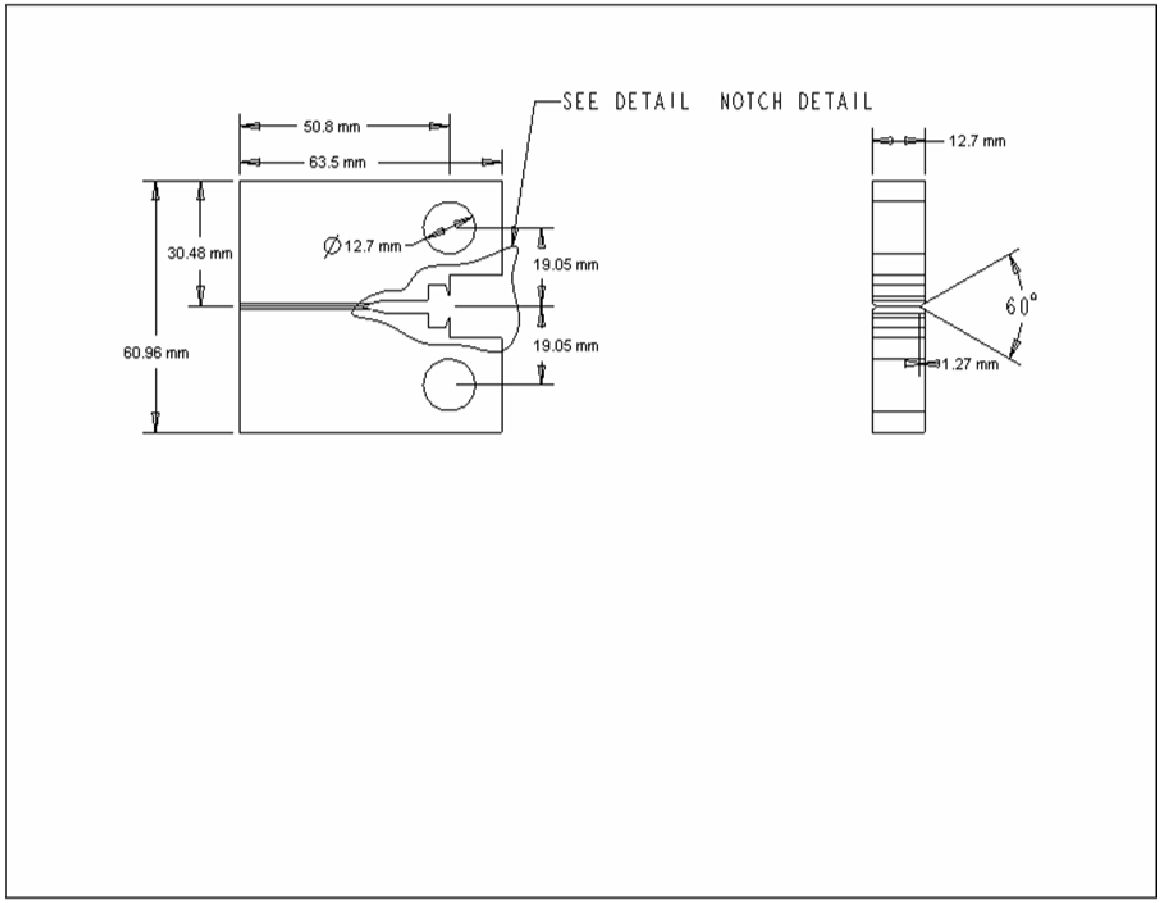

Figure B-1: Drawing of J-integral sample used for toughness tests.

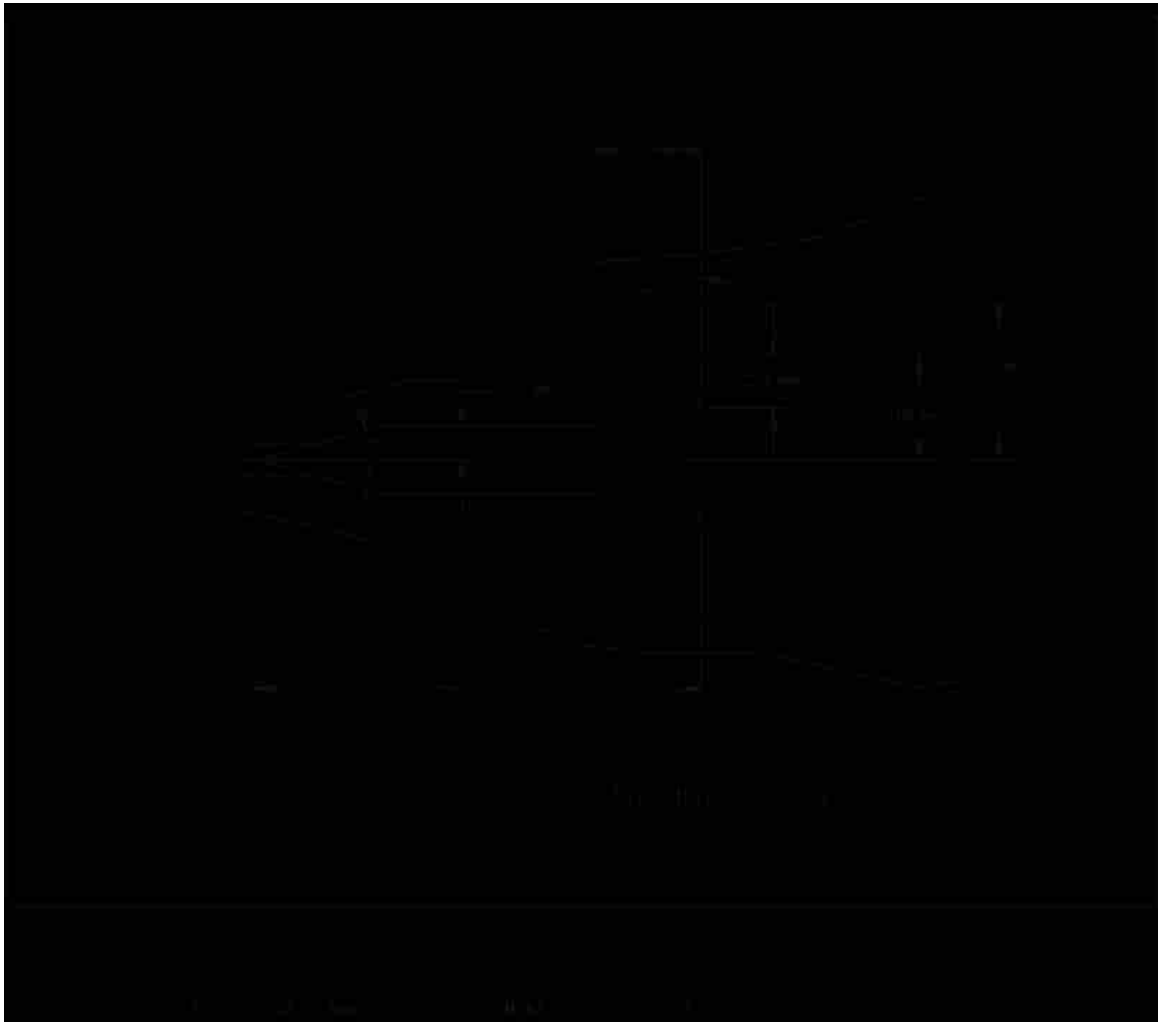

Figure B-2: Detail of notch in J-integral specimen.

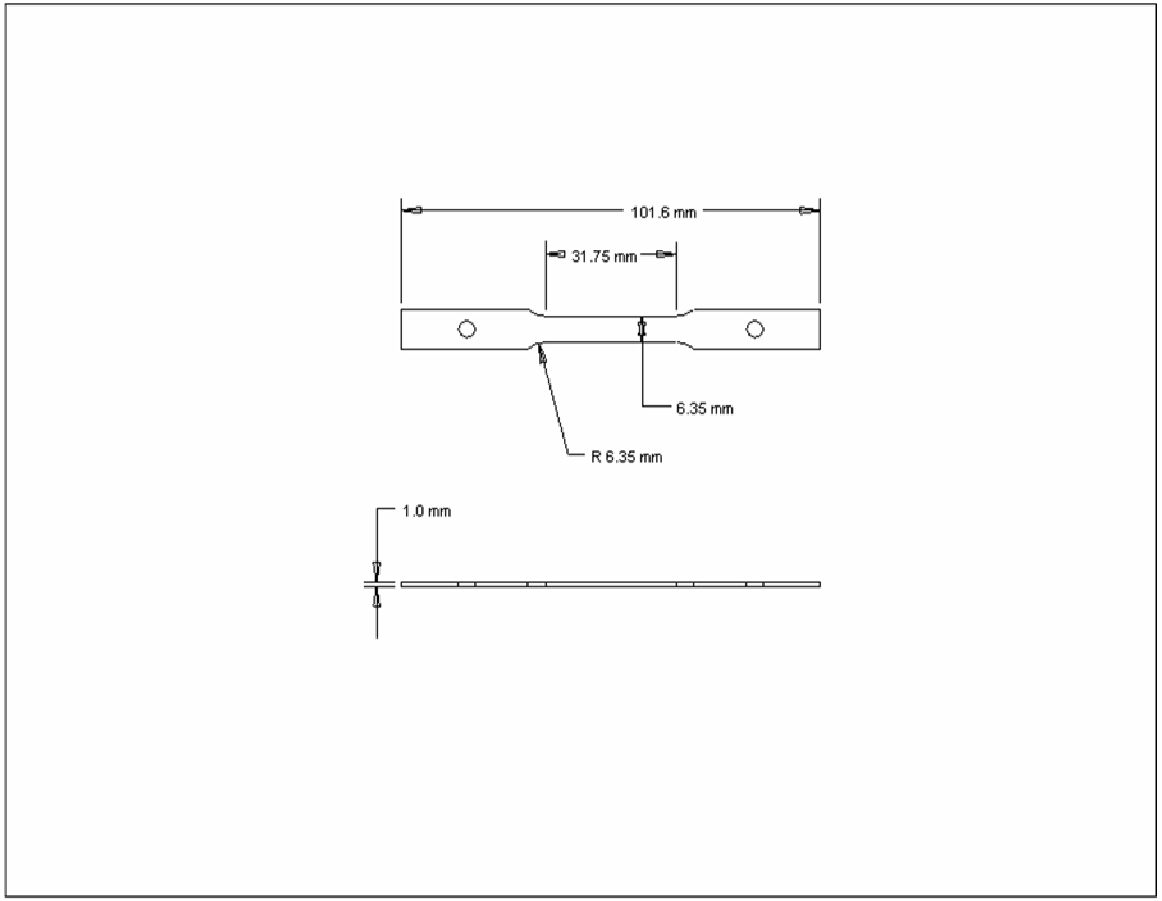

Figure B-3: Tensile sample dimensions.

Appendix C. Resistance Curves

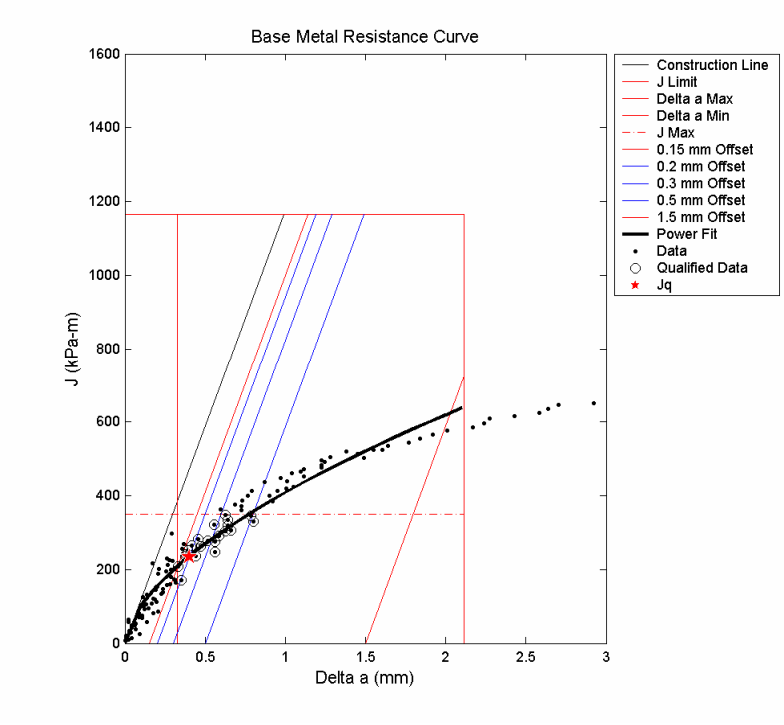

Figure C-1: Base metal resistance curve.

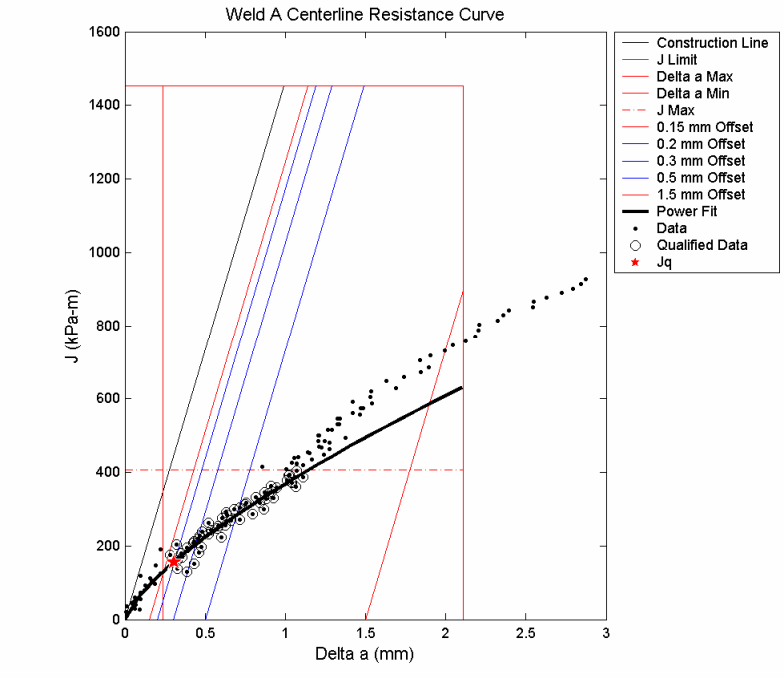

Figure C-2: Weld A, centerline resistance curve.

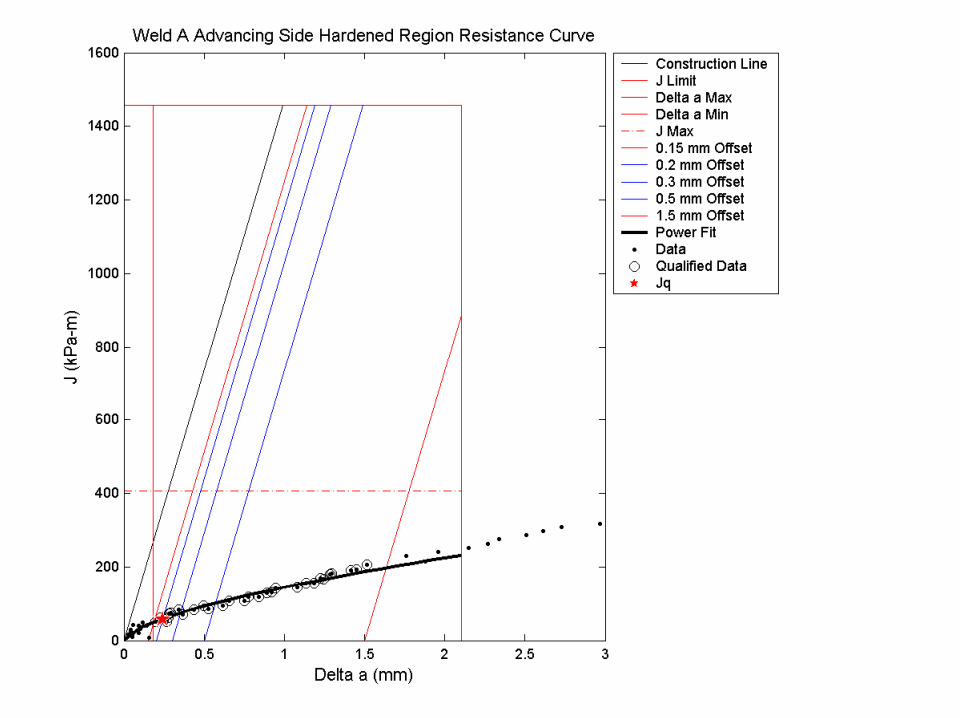

Figure C-3: Weld A, advancing side hardened region resistance curve.

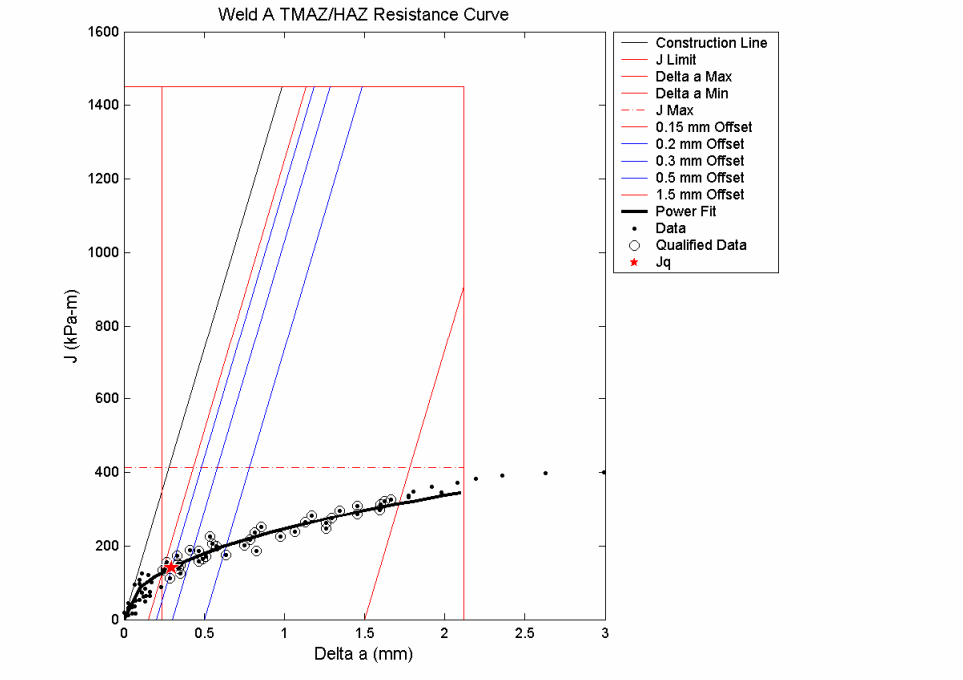

Figure C-4: Weld A, TMAZ/HAZ resistance curve.

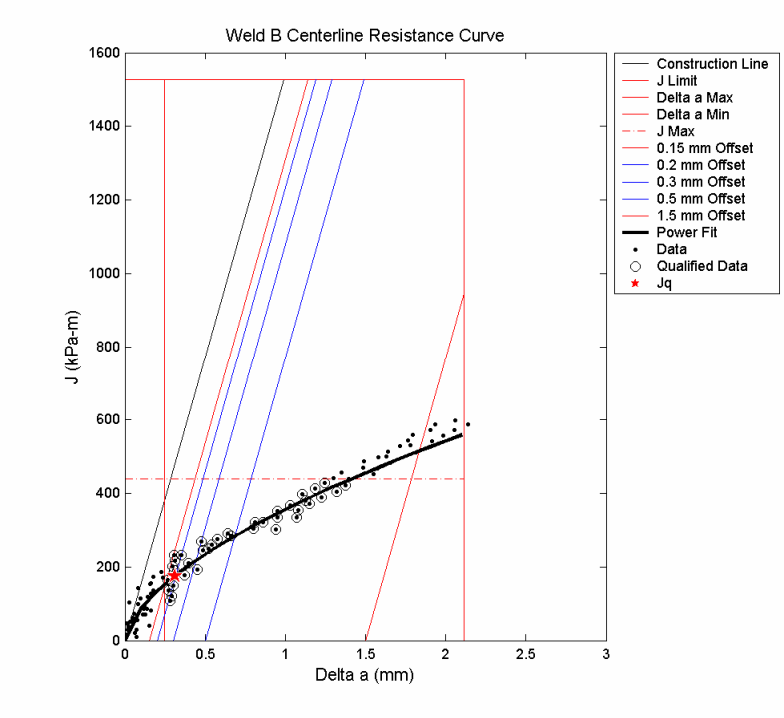

Figure C-5: Weld B, centerline resistance curve.

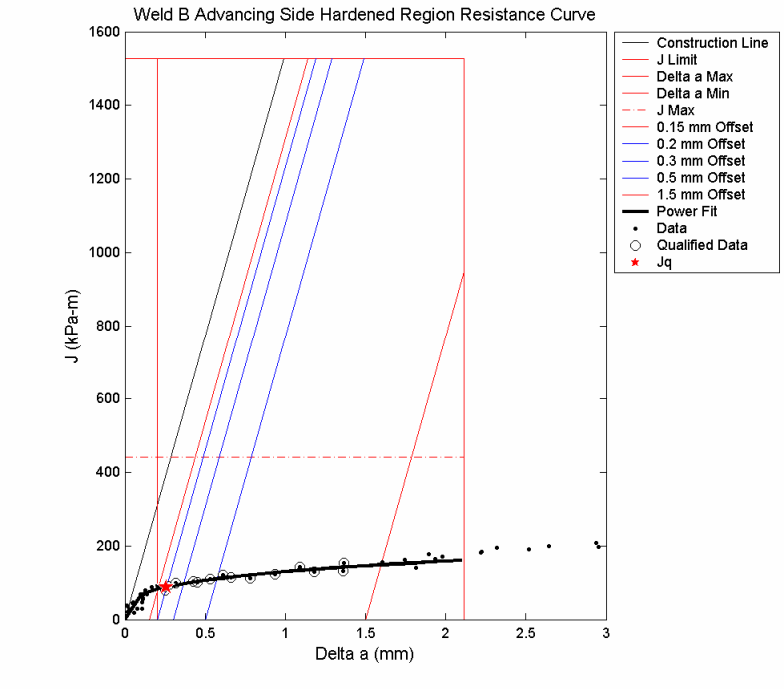

Figure C-6: Weld B, advancing side hardened region resistance curve.

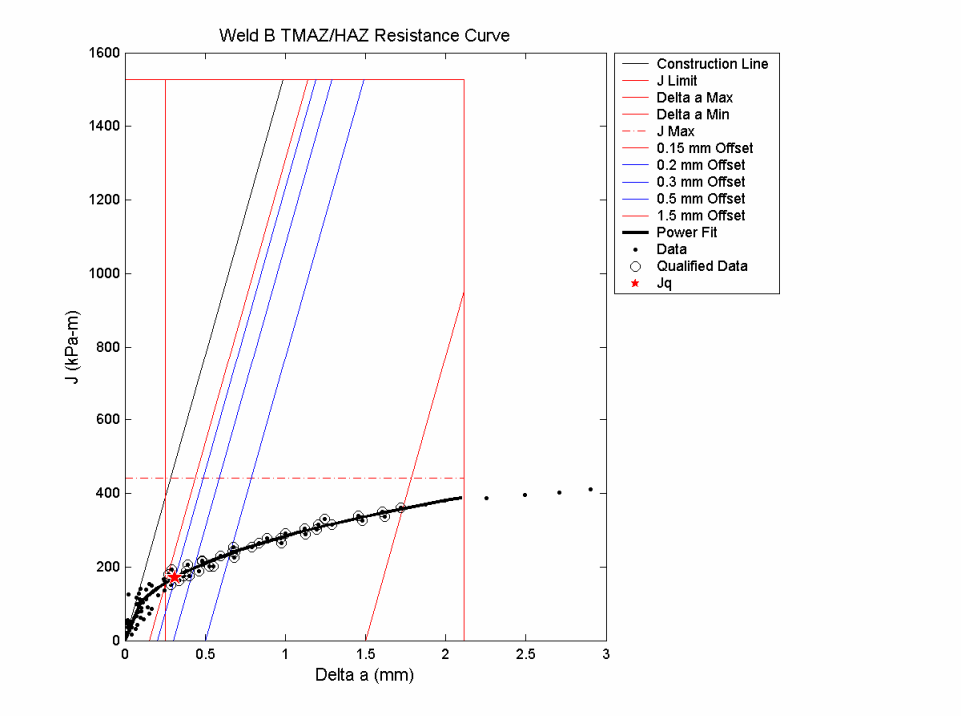

Figure C-7: Weld B, TMAZ/HAZ resistance curve.

Appendix D. Estimation of Yield Stress from Hardness

In order to resolve differences in yield stress between individual crack planes that the reported tensile data (Figure 3-1) does not provide, the through thickness Vickers hardness measurements from Figure 3-4 needed to be manipulated to estimate yield stress. This appendix describes the process that was followed in order to accomplish this estimation

Yield stress is estimated from Vickers hardness in Equation (6) [12].

$$\sigma_y = DPH \times \frac{1}{3}(0.1)^n \quad \textbf{(6)}$$

DPH is the Vickers hardness, and n is the strain hardening coefficient.

Strain hardening coefficients were estimated from the stress-strain records of the tensile samples reported in section 3.1. Stress-strain data between the yield and ultimate strengths were fit with a power curve. The exponent in this curve fit is the strain hardening coefficient and are reported in Table D-1.

Table D-1: Estimated strain hardening coefficients for tensile samples.

Sample Number	Base Metal	Weld A	Weld B
1	0.03	0.05	0.05
2	0.03	0.04	0.04
3	0.03	0.06	0.04
4	0.03	0.15	0.07
5		0.13	0.13
6		0.11	0.12
7		0.13	0.09
8		0.12	0.09

To simplify the process of correlating the through thickness locations of the tensile samples to locations of hardness measurements, strain-hardening coefficients were averaged for the base metal, and for the first and second weld passes of each weld. These are presented in Table D-2.

Table D-2: Average coefficients for base metal and individual weld passes for welds A and B.

Base Metal	Weld A		Weld B	
	2nd Pass	1st Pass	2nd Pass	1st Pass
0.03	0.05	0.13	0.05	0.11

Equation (6) was then simplified to be the Vickers hardness multiplied by a factor for the base metal, and for the first and second weld passes for each weld. Factors are reported in Table D-3. This factor includes unit conversions necessary for converting Vickers hardness units (kgf/mm^2) to stress (MPa).

Table D-3: Factors for converting to yield stress.

	Base Metal	Weld A		Weld B	
		2nd Pass	1st Pass	2nd Pass	1st Pass
DPH x	3.050699	2.913395	2.423257	2.913395	2.537461

Estimates of yield stress were then made multiplying the Vickers hardness by the factor in Table D-3 for the corresponding location.